

Research paper

# A qualitative analysis of ubiquitous regulatory motifs in *Saccharomyces cerevisiae* genetic networks

Erika T. Camacho<sup>a,\*</sup>, Anca Radulescu<sup>b</sup>, Stephen Wirkus<sup>a</sup>, Pamela A. Marshall<sup>a</sup><sup>a</sup>School of Mathematical & Natural Sciences, Arizona State University, 4701 W. Thunderbird Rd, Glendale, AZ 85306, USA<sup>b</sup>Department of Mathematics, SUNY - New Paltz, 1 Hawk Drive, New Paltz, NY 12561, USA

## ARTICLE INFO

## Article history:

Received 22 January 2018

Revised 10 August 2018

Accepted 3 September 2018

Available online 20 September 2018

## Keywords:

Bifurcation

Gene network

Recurrent neural network

## ABSTRACT

This work examines bistability and multistability within a Recurrent Neural Network model (RNN) for a 2-node and 3-node system under many different regulation scenarios. We determine parameter regions where there is bistability, multistability, or other stable modes in the expression states of the systems described by this network model. Our results show that although bistability can be generated with autoregulation it is also the case that both autorepression or no autoregulation can yield bistability as long as a sigmoidal behavior is present. Additionally, our results show the importance of considering more than a single connection when inferring a network as the observed biological result is averaged over many outcomes, which has implications for many algorithms that infer gene regulatory networks using the RNN models.

© 2018 Elsevier B.V. All rights reserved.

## 1. Introduction

Systems biology has made considerable advancements in a short period of time. Over the course of the last fifteen years, the field has emerged from the hopeful identification of one gene possibly affecting another gene to the classification of thousands of genes within networks. This emergence has led to the identification of transcription factors, network motifs, regulatory networks, and more [29]. Because so much has been done, we can begin to explore extremely complex questions in systems biology, from cell differentiation to regulation in very large networks of genes. One approach has been to identify transcription factors and network motifs in order to infer an architecture through experimental observation using mathematical algorithms. However, the inference of gene networks presents huge challenges mainly because of the tens or hundreds of free parameters that are difficult and in some cases impossible to measure directly yet must be estimated to infer the network structure [1,13]. Our work is additionally motivated by known networks and knockout experiments where a particular gene is deleted as well as knowledge that even a single sigmoidal equation can give rise to bistability. Thus it is crucial to understand the implications of node connections and choices of parameter values [35,38]. Our results will show that incorrectly estimating a single vs. two-way connection or ignoring the possibility of multistability may lead to ineffective inferring the network structure [17].

Numerous mathematical models have been used to model gene regulatory networks, the three prominent ones being the S-system (SS) model, the Hill kinetics model, and the Recurrent Neural Network model (RNN) [34]. Positive feedback

\* Corresponding author.

E-mail addresses: [erika.camacho@asu.edu](mailto:erika.camacho@asu.edu) (E.T. Camacho), [radulesa@newpaltz.edu](mailto:radulesa@newpaltz.edu) (A. Radulescu), [swirkus@asu.edu](mailto:swirkus@asu.edu) (S. Wirkus), [pamela.marshall@asu.edu](mailto:pamela.marshall@asu.edu) (P.A. Marshall).

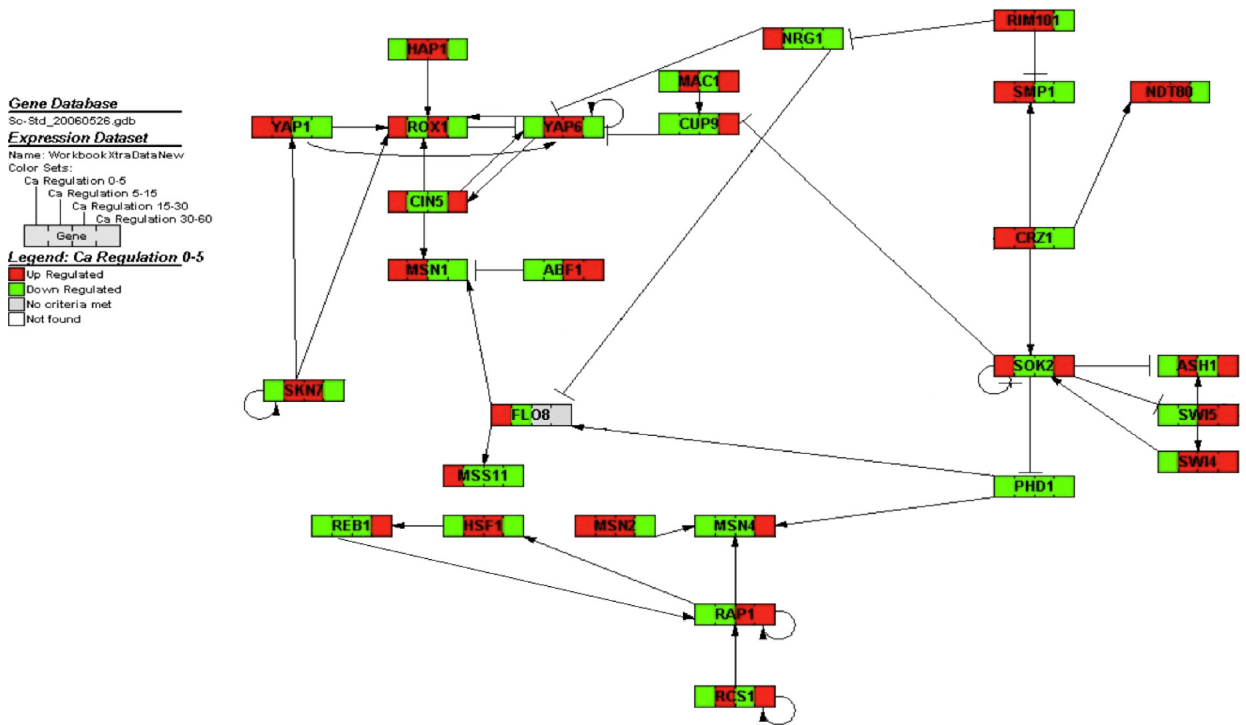


**Fig. 1.** Gene regulatory subnetwork of *Saccharomyces cerevisiae* that is sensitive to calcium. In this network arrows represent activation and bars represent repression. The rectangular-boxes corresponds to various genes as indicated by their names/ labels. The colors correspond to up regulation (red) and down regulation (green) of each gene within four different intervals; 0–5, 5–15, 15–30, and 30–60 min. Data provided by M.S., Cyert and supplemental documents in [33]. (For interpretation of the references to color in this figure legend, the reader is referred to the web version of this article.)

interactions defined by nonlinear sigmoidal transcription functions in a Hill type model have been observed to generate distinct epigenetic states [12]. This requirement for the existence of biological switches inducing multiple stable states in a system support the important fact that in actual molecular networks positive feedback interactions can lead to two stable gene profiles where the same cellular environment and conditions can result in two distinct gene expression states. In using a model to infer a gene network it is important to know when a specific gene in the network is likely to respond in such different ways. While [12] draws conclusions about the key role played by autoregulation in bistability and multistability for the Hill model, we focus on the RNN due to its wider applicability and popularity for inferring gene expression networks and identifying gene regulatory connections [34].

A simplified version of the symmetric archetypes of regulators that connect in a symmetric 2-node model without delay or external input was previously considered by Blasi et al. [3]. However, asymmetries as well as delay and external input are always part of a real biological genetic system as not all transcription processes are instantaneous and the experimental data collection can result in errors. Furthermore delay and external input are always considered as possibilities when inferring networks via the RNN [39–43]. Thus, our work extends these results by examining both asymmetric connections and external input. The consideration of these elements even within the symmetric case resulted in richer dynamics and the possibility of multistability and other stable modes.

Our small scale analysis for determining the number of stable states of these building blocks of the larger network is important because it allows us to infer the minimum possible number of stable states in the large scale network in which this small network is embedded. This provides the foundation for a better understanding of the predicted gene expression dynamics by the RNN models. As pointed out by Ingram et al. [15] knowing how things are connected is not enough to gain significant insight into the overall predicted dynamics.

The process of extracting or predicting regulatory information is technically difficult in systems biology and this difficulty increases with the model's nonlinearity and complexities [5,24]. The evaluation function of many of the optimization methods to infer a regulatory network focuses on reproducing a given time-course and when global stability is the premise of the selected method, it may converge to any of the multiple local minima thus rarely attaining the correct skeletal structures even in the presence of extensive time-series data [1,8,13,17]. For researchers who utilize the RNN model to infer networks, our results can provide guidance in determining if their system can potentially have more than one stable state based on the structure of a single or a few key known motifs in the system [27]. With 64 possible combinations of connections in the 2-node model and 19,683 possible combinations in the 3-node model, knowing conditions under which multistability exists is important. Our work can also guide their choice of allowable parameter regimes if it is known that a particular

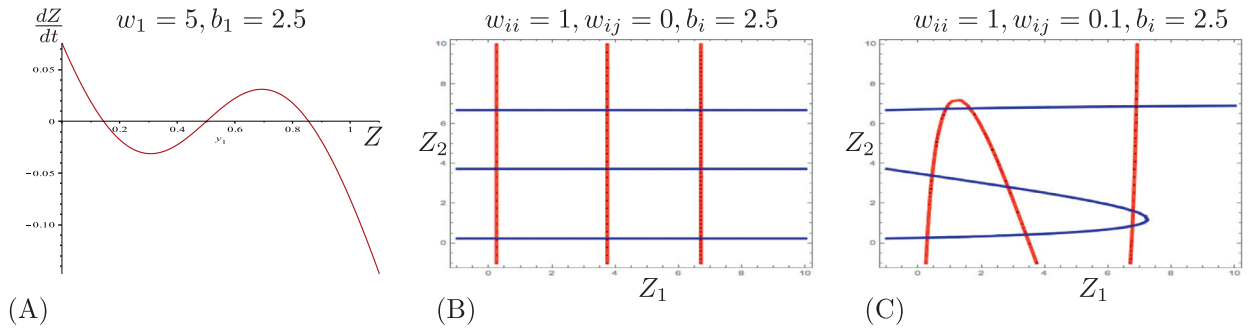


**Fig. 2.** Equilibria in 1-node and 2-node models of Results 1 and 2. (A): Phase line for a single node with 3 equilibria (located at the horizontal intersections), two of which are stable; see Result 1. Here,  $k_1 = d_1 = 1$ . (B): Nullclines (horizontal and vertical lines) for the uncoupled two-node system with nine equilibria, four of which are stable (located in the diagonal outermost intersections); see Result 2. Here  $k_i = 7$  and  $d_i = 1$ . (C): Nullclines for weakly coupled two-node system with nine equilibria, four of which are stable; see Result 2. Here  $k_i = 7$  and  $d_i = 1$ .

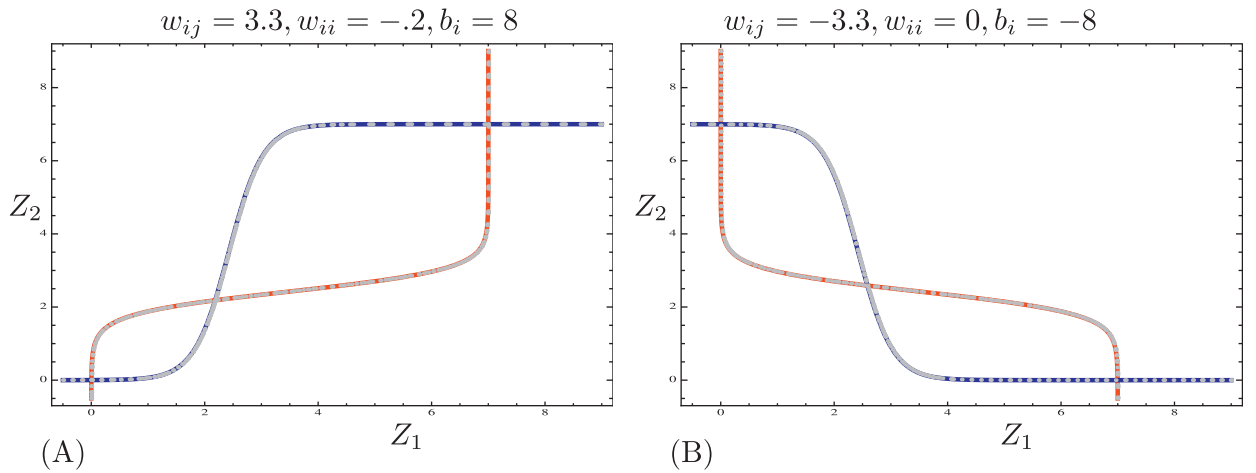


**Fig. 3.** Bistability without autoactivation. For both plots,  $k_i = 7, d_i = 1$ . (A): Two stable solutions for a system with negative feedback (autorepress-autorepress) where  $w_{ii} = w_{jj}$ , and with the same type of cross-regulation (activation-activation) where  $w_{ij} = w_{ji}$ . Stable solutions are located at top-right and bottom-left intersections. In an autorepress-autorepress system changing the signs of  $w_{ij}$  and  $b_i$  yields bistability when the cross-regulation in both directions is repression. (B): Two stable solutions located at top-left and bottom-right intersections for a no autoregulation system,  $w_{ii} = w_{jj} = 0$ , with (repression-repression) cross-regulation,  $w_{ij} < 0, w_{ji} < 0$ . Changing the signs of  $w_{ij}$  and  $b_i$  yields bistability when the cross-regulation in both directions is activation.

gene or genes (within the inferable network) exhibit bistable or multistable gene expression profiles. Our work supports the work of [13] and others who argue against focusing solely on parameter estimation when an understanding of the system under investigation is tentative or incomplete. By knowing *a priori* if the network exhibits bistable or multistable states, researchers inferring networks with RNN can better select their optimization subroutine to infer the network. We note in passing that the above comments on the choice of optimization method that may not result in the most accurate parameter values, besides benefiting from the results and insights of this current work, may also benefit from global optimization by direct search [18].

*A Calcium-sensitive network in Saccharomyces cerevisiae*

Many known gene regulatory networks exist in the literature. However, as another illustration of the variety of connections in ubiquitous regulatory motifs, we constructed a novel gene regulatory network of the most well-studied genes known to induce and repress other genes in response to calcium changes in the cytosol in *Saccharomyces cerevisiae* based on data from the literature; see Fig. 1. A full network of all transcription factors that interact in response to cytosolic calcium is much beyond the scope of this initial analysis. The set of genes in the network module, illustrated in Fig. 1, were selected because of their important roles and influences in a calcium environment and we utilized known datasets of transcriptional induction and degradation to identify regulatory motifs that were shared between gene networks. The investigation of calcium-sensitive transcription factor pathways can lead to a better understanding of the functioning regulatory network that exists within the yeast cell and how the yeast cell reacts to this calcium stimulus. To create the network, we selected the calcium-sensitive genes and then deciphered their corresponding connections through an intensive literature review and data mining. We reviewed several papers that suggest connections between the chosen genes that are most susceptible to

calcium. From there, genes were identified as either promoters or repressors of the other genes within the module/network under consideration. The master genes promoting or inhibiting the production of transcription factors in charge of initiating the transcription and translation processes of certain genes in our yeast network were identified as regulators. The genes to which the transcription factors bind in their respective DNA sites were identified as target genes.

The transcription process results in the production of mRNA products which are then translated into protein that modulates cellular functions under various environments including cell survival, functioning, and growth. As such both the datasets and RNN model utilized in this work consider the gene mRNA as a way to quantitatively and qualitatively measure the expression levels of the genes in the network. Fig. 1 identifies the network we developed and utilized for this analysis. CRZ1 is the key regulator of gene expression in calcium homeostasis, as it is dephosphorylated in response to cytosolic calcium. This then causes the protein to move into the yeast nucleus where it binds to DNA and stimulates transcription to respond to calcium [33]. Calcineurin acts through the CRZ1/TCN1-encoded transcription factor to regulate gene expression in yeast [33]. CRZ1 protein in turn stimulates the transcription of a wide array of genes, including SOK2 [45]. This gene in turn feeds into a network of transcription factors, all regulating each other in a complex network as explained by Lee et al. [20] with additional interactions as outlined in [2,16,19,31,45]. Each gene node is generally both a protein transcription factor that binds to DNA and stimulates transcription as well as a target itself (except for a few such as HAP1) that is regulated by transcription factor(s) binding to and inducing or repressing its own mRNA synthesis. We will interpret our model results in the context of this network.

## 2. Mathematical model

As mentioned earlier, we focus on the RNN model given its robustness and that it still takes into account the combinatorial aspects of gene regulation acting in tandem on a target gene within a network [3,21–23,34,36,39–43]. The resulting gene profiles of a network composed of  $n$  interacting genes are measured in the amount of respective mRNA levels and given by the governing equations

$$\frac{dZ_1}{dt} = \frac{k_1}{1 + \exp(\sum_{j=1}^n -w_{1j}Z_j + b_1)} - d_1Z_1, \quad (1)$$

$$\frac{dZ_2}{dt} = \frac{k_2}{1 + \exp(\sum_{j=1}^n -w_{2j}Z_j + b_2)} - d_2Z_2, \quad (2)$$

$$\vdots$$

$$\frac{dZ_n}{dt} = \frac{k_n}{1 + \exp(\sum_{j=1}^n -w_{nj}Z_j + b_n)} - d_nZ_n, \quad (3)$$

In Eqs. (1)–(3), the change in the amount of mRNA,  $Z_i$  of the target gene  $i$  for  $i = 1, \dots, n$ , results from the combinatorial effects of its regulators, gene  $j$  for  $j = 1 \dots n$ , which may include autoregulation, and the target gene  $i$  natural degradation. The kinetics of this gene expression network are influenced by the parameters. Here  $k_i$  is the maximum rate of expression of gene  $i$ ,  $w_{ij}$  are the regulatory weights,  $b_i$  is the unspecified external input that exists outside of the regulatory genes (and can also be considered as a measure of delay in the transcription process of gene  $i$ ), and  $d_i$  is the half-life of gene  $i$ . The regulatory weights  $w_{ij}$  are a measure of the amount of influence or affinity of the transcription factor, produced by the regulator gene  $j$ , to bind with a promoter region of the target gene  $i$  and initiate the production of  $Z_i$ . For target gene  $i$  not being regulated by gene  $j$ , the value of the corresponding regulatory weight,  $w_{ij}$ , is 0. With the negative sign explicitly included in the regulatory terms  $w_{ij}Z_j$  in (1)–(3), we see that if  $w_{ij} > 0$  then the regulator gene  $j$  is an activator and if  $w_{ij} < 0$  then it is a repressor. The interconnected kinetics of this biological system are such that at any given time a target gene may also be acting as a regulator of another gene or itself.

In the remainder of this work, we address 1) the parameter configuration allowing for bistability or multistability in gene profiles of various key regulatory motifs, 2) the maximum possible number of stable gene profiles within these motifs, 3) additional stable modes that may be present in the gene profile, and 4) the regulatory interactions that arise from these qualitative dynamics. Mathematically, stable equilibrium (or steady state) solutions of the network dynamics illustrated by Eqs. (1)–(3) correspond to the underlying stable gene expression profiles (or expression states) of this network. Having two or possibly more stable gene expression profiles is ubiquitous in certain networks such as [10,28,30,32]. Thus it is important to thoroughly investigate the regulatory interactions and the configuration of parameters that give rise to multistable (including bistable) expression states and thereby determine which prototype motifs are consistent with what we know. While this was investigated by Blasi et al. [3] for certain symmetric cases of the 2-node and 3-node motifs, the authors of this current work have not seen a complete analysis in the literature for the RNN networks for the non-symmetric cases. Result 1 is stated for one node and is then used in Result 2 for the 2-node system. Both are then used in Result 3 for the 3-node system. Additionally, analytical and numerical (via MATCONT) bifurcation analysis examines other stable modes of the systems [6,7].

### 3. Multistable solutions

We are interested in understanding how changes in our parameter set give rise to different long term gene profiles. In the case of our yeast network that is susceptible to calcium, it responds in a qualitatively different manner in a calcium environment versus a calcium-free environment leading to different gene profiles of most of the genes involved [33]. Bifurcation analysis will allow us to investigate the number of stable gene profiles that are possible for certain parameter values of a 2-node and 3-node subnetwork. This is extremely important given that most of the inferred yeast genetic networks in the current literature contain vastly different parameter values for the weights, the maximal expression rates and degradation rates and that many algorithms for finding these weights only focus on optimization without concern for the potential of multiple stable states [4,13]. In particular, the values for the maximal expression rates  $k_i$  and degradations rates  $d_i$  obtained through the process of inferring the network are in some cases not biologically possible even when the inferred network is based on extensive microarray data, such as in [39–43]. For example, in [43]  $k_i$  values range from 0.4 to 44 molecules/min, a gross overestimate of transcription rate in *S. cerevisiae*. Maximal expression rates have been generated from many experiments utilizing *S. cerevisiae* and these expression rates generally vary from 1 to 600 transcripts per cell cycle [26]. The mRNA synthesis rate of ASH1 after stress has been calculated to be 43.27 mRNA molecules made/cell/cell cycle, which biologically means that less than 0.5 mRNA molecule is made per minute per cell (assuming a cell cycle of 90 min) and to be 1.2 molecule/hr in non-stressed cells [14,26]. Other experiments, have demonstrated that the transcription rate for a yeast gene is 0.05 to 0.084 transcripts/min/cell [9]. Thus, yeast in general makes mRNA at a low level per cell and applying the RNN model to inferring the network without knowledge of potential qualitative behavior can lead to significant overestimated values for  $k_i$ . The parameter  $d_i$  is also a crucial component of the expression profile that may be inaccurately estimated. In [43],  $d_i$  ranged from 6.7 to 0.2, which translates into parameterized half-lives of 0.1 min–3.46 min. Half lives of *S. cerevisiae* mRNA are well described by many research studies. For example, the half life of SOK2 is 15 min and ASH1 is 22 min which yield  $d_i$  of 0.05 and 0.03 respectively [11]. In yeast, all half lives of mRNA have been calculated to be between 3 and 100 min depending on the gene and environmental conditions, with an average of around 23 min [44]. Thus, the estimated  $d_i$  values of [39–43] fall far out of the actual biological range of *S. cerevisiae*. The purpose of this work is to show that systematically allowing additional connections guided by knowledge of multistability may help in obtaining more accurate parameter values.

#### 3.1. Two nodes

We consider the subnetwork made up of two nodes, cf. (1)–(2), with its governing dynamics given by

$$\frac{dZ_1}{dt} = \frac{k_1}{1 + \exp(-w_{11}Z_1 - w_{12}Z_2 + b_1)} - d_1Z_1 \quad (4)$$

$$\frac{dZ_2}{dt} = \frac{k_2}{1 + \exp(-w_{21}Z_1 - w_{22}Z_2 + b_2)} - d_2Z_2. \quad (5)$$

As before,  $Z_i$  for  $i = 1, 2$ , is the amount of mRNA of gene  $i$ , which depends on its specific  $k_i$ ,  $w_{ij}$ ,  $b_i$ , and  $d_i$ , all previously defined, and where regulator gene  $j$  is an activator when  $w_{ij} > 0$ , and is a repressor when  $w_{ij} < 0$ . While seemingly straightforward, this important analysis has not been systematically studied. Some work has been done previously on the 2- and 3-node systems for very specific cases but the analysis and results were limited to a subset of the “symmetric” cases [3]: equal expression rates were considered, the degradation rates were set equal to one, the external input in the data was set to zero, and autoregulation was always considered. We briefly present the equations of [3] in order to set the context of our results. More specifically, [3] considered a reduced symmetric case of (4)–(5) with  $w_{ii} = 1$ ,  $|w_{ij}| = |w_{ji}| \in (0, 1]$ ,  $k_1 = k_2$ ,  $d_i = 1$ , and  $b_i = 0$  for  $i = 1, 2$ . Depending on the values of the parameters, they observed 1, 3, or 5 equilibrium solutions. Before analyzing the more general equations (4)–(5), we compare the form of these equations with those in [3] via a non-dimensionalization of our system. We rescale (4)–(5) by redefining our parameters and variables as follow:

$$c_1 = \frac{w_{12}}{w_{22}}, \quad c_2 = \frac{w_{21}}{w_{11}}, \quad \delta = \frac{d_2}{d_1}, \quad \kappa_1 = \frac{w_{11}k_1}{d_1}, \quad \kappa_2 = \frac{w_{11}k_2}{d_1}$$

$$y_1 = w_{11}Z_1, \quad y_2 = w_{22}Z_2, \quad \text{and} \quad \tau = d_1t.$$

Substituting these and writing Eqs. (4)–(5) in terms of our new variables yields our non-dimensional system

$$y_1' = \frac{\kappa_1}{1 + \exp(-y_1 - c_1y_2 + b_1)} - y_1 \quad (6)$$

$$y_2' = \frac{\kappa_2}{1 + \exp(-c_2y_1 - y_2 + b_2)} - \delta y_2, \quad (7)$$

where the rate of change of the rescaled mRNA levels  $y_1$  and  $y_2$  are now in terms of our new time variable  $\tau$  as well as the parameters  $b_i$ ,  $c_i \in \mathbb{R}$  and  $\kappa_1, \kappa_2, \delta > 0$ . Given that  $b_i$  is defined as the unspecified external input to the regulators but

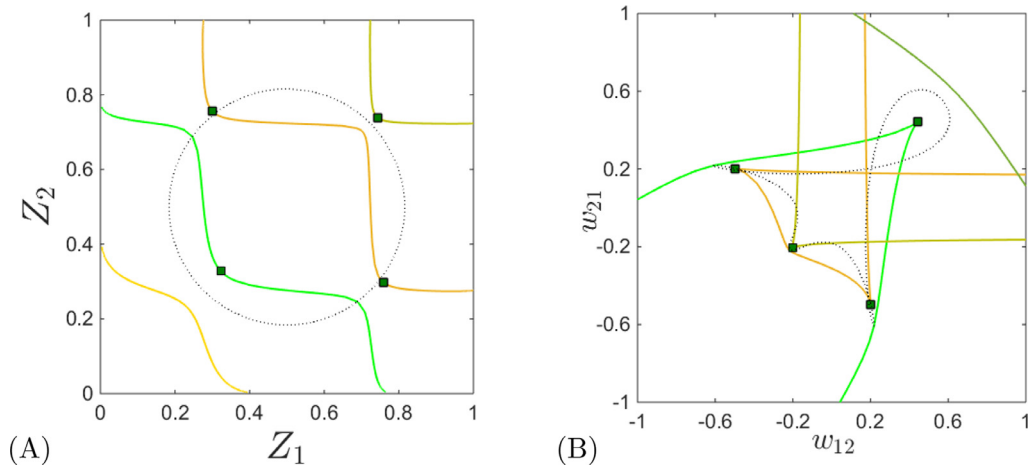


**Fig. 4.** Bifurcation curves with respect to  $w_{12}$  and  $w_{21}$ . The graphs show the evolution of Saddle Node curves (plotted in various shades of green and yellow), as  $w_{12}$  and  $w_{21}$  are varied. The Neutral Saddle curve computed analytically is shown as a thin dotted curve. (A): Bifurcation curves with respect to  $w_{12}$  and  $w_{21}$ , shown in the  $(Z_1, Z_2)$  phase plane. (B): The same bifurcation curves are shown in the  $(w_{12}, w_{21})$  parameter plane. In both graphs, the green squares mark the Cusp points (tangent intersections of Saddle Node branches). A detailed account of the behaviors between the bifurcation curves is shown in Appendix A. The other parameters were fixed to:  $w_{11} = w_{22} = 5$ ,  $b_1 = b_2 = 2.5$ ,  $k_1 = k_2 = 1$  and  $d_1 = d_2 = 1$ . (For interpretation of the references to color in this figure legend, the reader is referred to the web version of this article.)

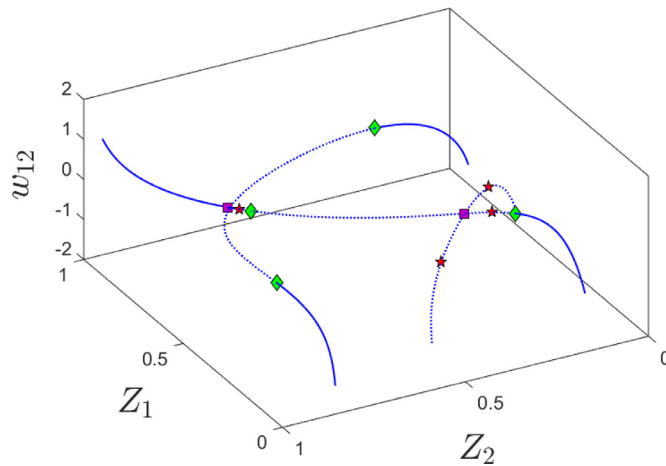


**Fig. 5.** Bifurcation diagram with respect to  $w_{12} = w_{21}$  (vertical axis). The graphs show the evolution and stability changes of the system’s equilibria in the  $(Z_1, Z_2)$  (horizontal) plane as the coupling parameter  $w_{12}$  is varied, for the symmetric case when  $w_{12} = w_{21}$ . The equilibria are shown as solid curves when they are stable, and as dotted curves when they are unstable. Saddle node bifurcations are shown as green diamonds, pitchfork bifurcations as purple squares, and neutral saddles as red stars. The other parameters were fixed to:  $w_{11} = w_{22} = 5$ ,  $b_1 = b_2 = 2.5$ ,  $k_1 = k_2 = 1$  and  $d_1 = d_2 = 1$ . (For interpretation of the references to color in this figure legend, the reader is referred to the web version of this article.)

acting on the target genes and that the mRNA from different genes can have vastly different half-lives,  $d_i$ , we consider our general system of equations (4)-(5) to be more realistic than the non-dimensionalized system (6)-(7) with  $\delta = 0$  and  $b_i = 0$  for  $i = 1, 2$ . While this non-dimensionalized system is still more general than the one in [3] as it includes the unspecified external inputs and degradation rates, it only illustrates some cases. For example, the non-dimensional equations only allow us to consider nodes in which both are governed by autoregulation, something that is rare in most gene networks and, in particular, the yeast gene network we consider (see Fig. 1) [2,16,19,31,45]. Hence we choose to consider the general system (4)-(5) in order to analyze the entire spectrum of all possible connections and parameter configurations. Results 1 and 2 that follow are for the general system (4)-(5) and include the results of [3] as special cases.

**Result 1:** Consider  $Z' = f(Z)$  for  $f(Z) = \frac{k_1}{1 + \exp(-w_1 Z + b_1)} - d_1 Z$  with  $w_1 > 0$  (autoactivator) and  $0 < Z < \frac{k_1}{d_1}$ . For any  $k_1, d_1 > 0$ , there exists  $b_1$  such that the system contains three equilibrium solutions. Moreover, the smallest and largest of these solutions are stable.

Single node: For very small  $Z$ , we have  $f(Z) \approx \frac{k_1}{1 + e^{b_1}} > 0$ ; for  $Z \rightarrow \frac{k_1}{d_1}$ , we have  $f(Z) < 0$ . We thus always have at least one root. The appearance of additional roots corresponds to the conditions  $f = \frac{df}{dZ} = 0$ , that is, the conditions for a saddle node

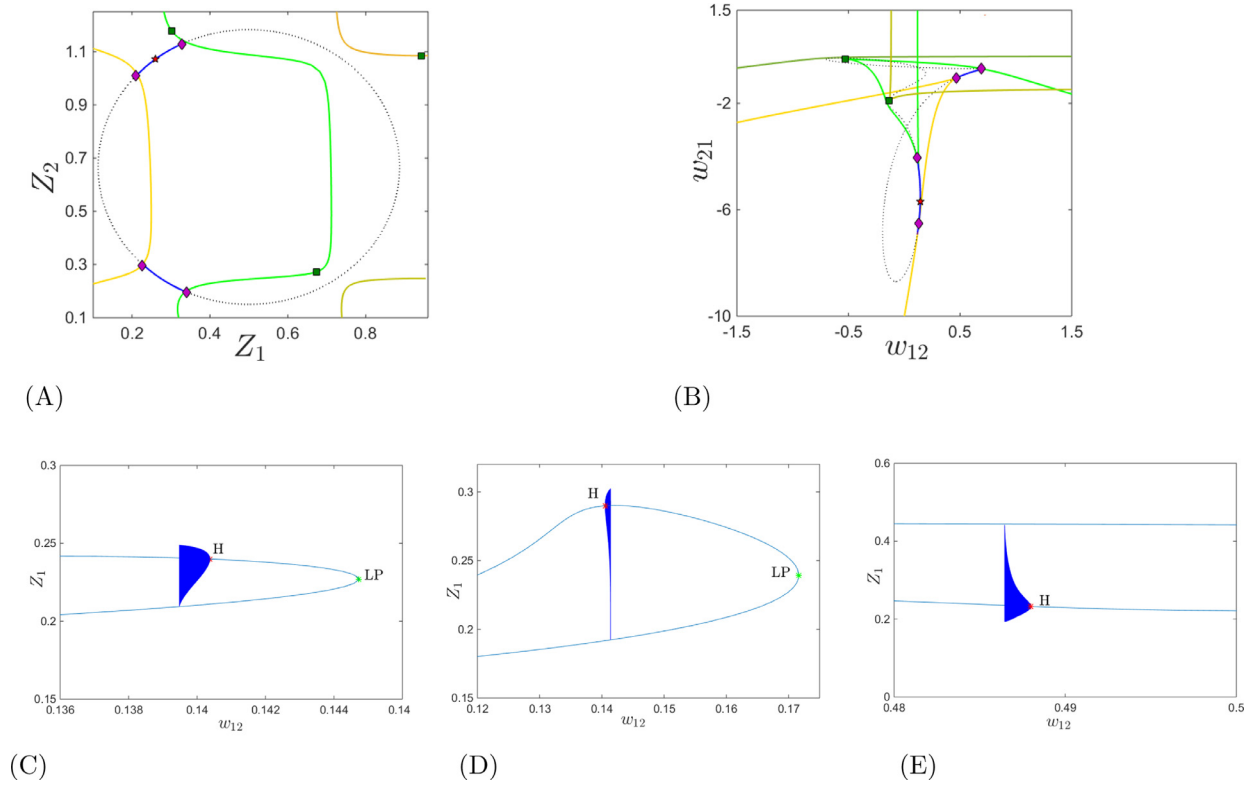


**Fig. 6.** Multistability and Hopf bifurcations with respect to  $w_{12}$  and  $w_{21}$ , in the nonsymmetric case  $d_1 \neq d_2$ . Fixed parameters:  $k_1 = k_2 = 1$ ,  $b_1 = b_2 = 2.5$ ,  $w_{11} = w_{22} = 5$ ,  $d_1 = 1$ ,  $d_2 = 0.75$ . (A): Bifurcation curves with respect to  $w_{12}$  and  $w_{21}$  traced in the  $(Z_1, Z_2)$  phase plane. Saddle Node curves are plotted as solid lines, in different shades of green and yellow, and the Hopf curves are plotted in blue solid lines. The Neutral Saddle curve is shown as a thin dotted line, connecting the Hopf portions. (B): The same curves shown in the  $(w_{12}, w_{21})$  parameter plane. In both panels, the colored markers show the co-dimension two bifurcations: Cusp points (tangential intersections of two Saddle Node branches) are marked with a dark green square; Bogdanov-Takens points (nondegenerate intersections of a Hopf curve with two Saddle Node branches and a Homoclinic curve) are marked with a purple rhombus; the Generalized Hopf point (intersection of the super-critical and sub-critical Hopf branches) is marked with a red star. Crossing the Hopf lower curve above the red star results in a subcritical Hopf transition from a stable equilibrium (left) to an unstable equilibrium surrounded by a stable cycle (right), as illustrated in panel C for  $w_{21} = -5$ . Crossing the Hopf lower curve below the red star produces a supercritical Hopf transition from an unstable equilibrium (right) to a stable equilibrium surrounded by an unstable cycle (left), as illustrated in panel D for  $w_{21} = -6$ . Crossing the Hopf upper curve also produces a supercritical transition from a stable equilibrium (right) to an unstable equilibrium surrounded by a stable cycle (left), as illustrated in panel E for  $w_{21} = -1$ . In all three panels C-E, we illustrate equilibrium curves traversing a Hopf bifurcation. Hopf points are marked with a red star (labeled H) and saddle node bifurcations are marked with a green rhombus (labeled SN) along the equilibrium curve (the SN point is out of range in panel E). In all three cases, the cycles are eventually destroyed via saddle homoclinic bifurcations. (C): Observed unstable limit cycles for  $w_{21} = -6$  as  $w_{12}$  varies. (D): Observed stable limit cycles for  $w_{21} = -5$  as  $w_{12}$  varies. More detail on these transitions is included in Figs. 7–8. (E): Observed stable limit cycles for  $w_{21} = -1$  as  $w_{12}$  varies. (For interpretation of the references to color in this figure legend, the reader is referred to the web version of this article.)

bifurcation. Eliminating  $b_1$  from the two conditions gives

$$w_1 d_1 \left( y_1 - \frac{k_1}{2d_1} \right)^2 + k_1 - \frac{k_1^2 w_1}{4d_1} = 0. \tag{8}$$

For any  $k_1, d_1 > 0$ , we see that  $w_1 > 0$  can always be chosen so that two positive roots,  $Z_{r1}, Z_{r2}$  exist. For definiteness, assume  $Z_{r1} < Z_{r2}$ . These  $Z_{ri}$  correspond to the location of the bifurcation to the left or right of the existing equilibrium; thus, at the bifurcation we will either have a double root at  $Z_{r1}$  and a single root to the right or a double root at  $Z_{r2}$  and a single root to the left. Together with this set  $\{k_1, d_1, w_1, Z_{ri}\}$ , we find that  $b_1 = w_1 Z_{ri} + \ln \left( \frac{k_1 - d_1 Z_{ri}}{d_1 Z_{ri}} \right)$  will satisfy  $f = \frac{df}{dZ} = 0$  (with  $i = 1$  corresponding to a saddlenode bifurcation when it occurs to the left of the existing root and  $i = 2$  for the bifurcation when it occurs to the right of the existing root). By continuity, we can find a small change in the parameters that will give three equilibria. Because  $f(0) > 0$  and  $f(\frac{k_1}{d_1}) < 0$ , phase line analysis confirms that the smallest and largest roots are indeed stable whenever there are three equilibria. See Fig. 2A.

**Result 2:** Consider the 2-node system (4)-(5):  $Z'_1 = f_1$  and  $Z'_2 = f_2$  with  $w_{ii} > 0$  for  $i = 1, 2$  (two autoactivators) and  $0 < Z_i < \frac{k_i}{d_i}$ . For any  $k_i, d_i > 0$ , there exists  $b_i$  and  $w_{ij}$  with  $i \neq j$  ( $i, j = 1, 2$ ) such that nine equilibrium solutions exist. Moreover, four of these equilibrium solutions are stable.

We consider two cases corresponding to  $w_{ij}$  zero and non-zero.

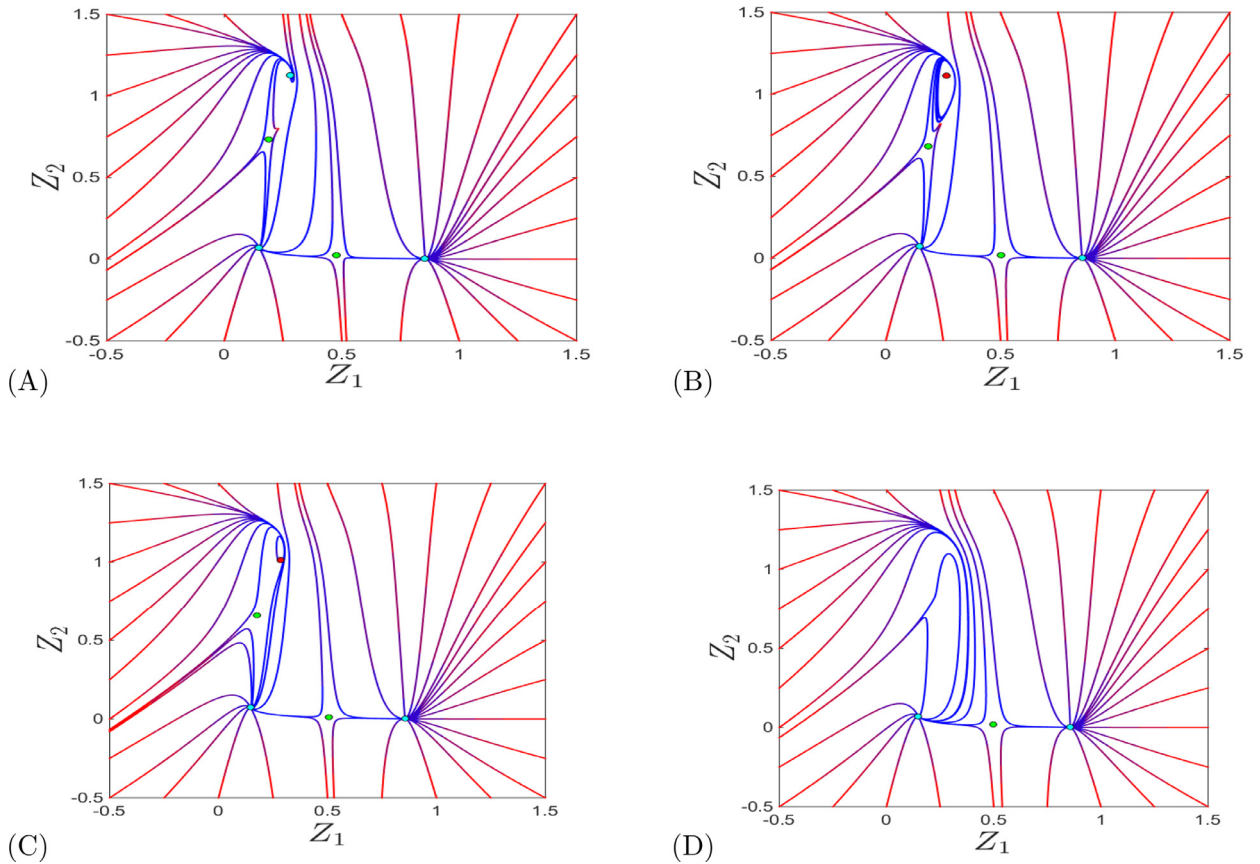


**Fig. 7.** Succession of phase plane diagrams focused on the region  $[-0.5, 1.5] \times [-0.5, 1.5]$ , as the system is undergoing the bifurcation sequence shown in Fig. 6D. The flow lines are shown in red-blue gradient, with the color representing time. (A): The system at  $w_{12} = 0.138$ , before the supercritical Hopf bifurcation; (B): The system at  $w_{12} = 0.141358$ , after the Hopf bifurcation, showing the attracting cycle; (C): The system at  $w_{12} = 1.42$ , after the homoclinic bifurcation, showing the cycle has been destroyed; (D): The system at  $w_{12} = 1.75$ , after the saddle node bifurcation where the repelling spiral and one of the saddles collide and disappear. The other fixed parameters:  $w_{11} = w_{22} = 5$ ,  $b_1 = b_2 = 2.5$ ,  $k_1 = k_2 = 1$ ,  $d_1 = 1$ ,  $d_2 = 0.75$ ,  $w_{21} = -5$ . (For interpretation of the references to color in this figure legend, the reader is referred to the web version of this article.)

Uncoupled system (corresponding to no cross-regulation): In the case of  $w_{ij} = 0$ , this reduces to Result 1 for each individual node considered independently. Thus there are a maximum of three equilibria mRNA-values,  $Z_i$ , for each node  $i$ , under certain parameter values and all the pair combinations obtained from these equilibria (one element in each pair from node 1 and the other from node 2) yield the equilibria when both are considered together as a system. When considering all possible combinations that result from these three equilibria values for each  $Z_i^*$ , nine total equilibrium pairs  $(Z_1^*, Z_2^*)$  result. Denoting the respective roots of each uncoupled equation as  $Z_{11}, Z_{12}, Z_{13}$  and  $Z_{21}, Z_{22}, Z_{23}$ , respectively, Result 1 gives that  $Z_{11}, Z_{13}, Z_{21}, Z_{23}$  are all stable. Thus  $(Z_{11}, Z_{21}), (Z_{11}, Z_{23}), (Z_{13}, Z_{21}), (Z_{13}, Z_{23})$  are stable in the  $(Z_1, Z_2)$  space. See Fig. 2B.

Coupled system (corresponding to cross-regulation): For the case when one or both of the  $w_{ij}$  are non-zero, we consider  $0 < w_{ij} \ll 1$  because together with  $Z_i^*$  being bounded this gives  $\exp(-w_{ij}Z_j) \approx C$  for the  $f_i$  equation with  $C \approx 1$ . Eliminating  $b_i$  from  $f_i = f'_i = 0$  again gives (8). Thus for any  $k_i, d_i > 0$ , we see that  $w_{ii} > 0$  can always be chosen so that two positive roots,  $Z_{ri1}, Z_{ri2}$  exist for each variable. (For definiteness, assume  $Z_{ri1} < Z_{ri2}$ . Analogous to the previous result, these  $Z_{rij}$  correspond to the location of the bifurcation to the left or right of the existing equilibrium; thus, at the bifurcation we will either have a double root at a  $Z_{ri1}$  and a single root to the right in the given variable or a double root at  $Z_{ri2}$  and a single root to the left in the given variable.) Together with the set  $\{k_i, d_i, w_{ij}, Z_{rij}\}$ , we find that  $b_i = w_1 Z_{rij} + \ln\left(\frac{k_1 - d_1 Z_{rij}}{cd_1 Z_{rij}}\right)$  is the corresponding  $b_i$ -value. By continuity, a small change in parameters can be found so that three equilibria exist for each variable with the smallest and largest again being stable. The combinations of the  $Z_{rij}$  give the nine equilibria. See Fig. 2C.

While Result 2 was shown for small coupling parameters  $w_{ij}$ , numerical evidence suggests that nine equilibria can exist even when  $w_{ij}$  is not small.

In the case of a single node autorepressor,  $w_{ii} < 0, w_{ij} = 0, i \neq j$ , it is easy to see that  $f'_i < 0$  for any choice of parameters and thus we will only have one equilibrium solution possible for a single equation. However, for a two-node system with both nodes exhibiting autorepression (i.e., an autorepressor-autorepressor system) we can find parameter values where up

to three equilibria exist, two of which are stable. In other cases involving autoregulation, we refer the reader the [Table 1](#) for possible stable equilibrium solutions. We note that in the case of no autoregulation in either node, there may be up to 3 equilibria, 2 of which are stable.

Result 2 thus shows that for any  $k_i$ ,  $d_i$  in the case of autoactivation, we can always find a  $w_{11}$ ,  $w_{22}$ ,  $b_1$  and  $b_2$  set such that we can have 4 stable equilibrium solutions (see [Fig. 2C](#)). This is again significant because in the RNN models, the  $w_{ij}$  and  $b_i$  are not determined directly from experimental data but are instead obtained through optimization algorithms via fitting the gene profile data to the computer simulation considering only one target gene (node) and one or two regulators at a time [[39–43](#)]. Having multiple stable solutions as described can lead to multiple local optimal solutions when trying to use an optimization algorithm to obtain a set of parameter values that yield acceptable gene profiles.

### Table Summary

We have also found parameter regimes of negative feedback or no feedback that can still give bistability; see [Fig. 3](#). When thinking of bistability as a progression switch this is important because while bistability may be more common when autoactivation is present, it is not necessary. [Table 1](#) gives a complete summary of when there exist multistable, bistable, or a unique stable solution in the 2-node system given by [Eqs. \(4\)–\(5\)](#). It includes total number of equilibria and the corresponding number of stable equilibrium solutions for this coupled system. In all cases, there is always at least one stable equilibrium solution. [Table 1](#) specifies under what types of regulatory interactions we might expect to find more than one stable solution. All possible interactions for the 2-node system are divided into six cases based on their respective autoregulatory activity determined by  $w_{ii}$  for  $i = 1, 2$  where autoactivation corresponds to  $w_{ii} > 0$ , autorepression corresponds to  $w_{ii} < 0$ , and no autoregulation corresponds to  $w_{ii} = 0$ . These six cases were further categorized based on their type of cross regulatory interactions  $w_{ij}$  and  $w_{ji}$ . If  $w_{12}w_{21} < 0$ , the cross-regulation is classified as “mixed” whereas if  $w_{12}w_{21} > 0$ , it is classified as “same”. If there is only one cross-regulatory connection in the 2-node system such that  $w_{12} = 0$  or  $w_{21} = 0$ , it is classified as “single only”. For “same” and “single only” cross-regulation both repression and activation yield the same number of total and stable equilibria. Thus the motif example diagrams in [Table 1](#) corresponding to the “mixed” and “single only” categories are only one of two possible sets of diagrams. However for brevity we only displayed the diagrams consisting of cross-activation even though the same results hold for cross-repression in every case in these two cross-regulatory categories.

In our results presented in [Table 1](#), we see the important role played by autoregulation. Specifically, in the case of autoactivation, we can always have an additional 1–3 stable equilibrium solutions beyond the normally expected stable equilibrium solution. While it may not be widespread in all genetic networks, we see autoregulation in many subnetworks within *S. cerevisiae*. For example, in the subnetwork shown in [Fig. 1](#) containing 28 genes, YAP6, SKN7, SOK2, RAP1 and RCS1 are autoregulating genes. Moreover, the presence of even a single autoactivation coupled in any way leaves open the possibility for at least two possible stable equilibrium solutions in the network. When a smaller system (such as our 2-node motif) is embedded in a larger system, the number of stable solutions in the entire network could be greater than or equal to the number of stable solutions in the smaller subsystem.

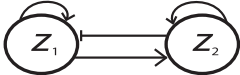
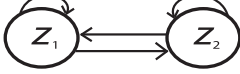
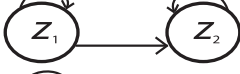
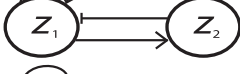
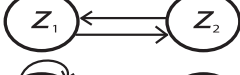
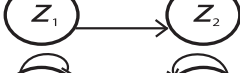
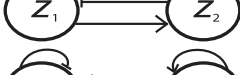
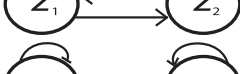
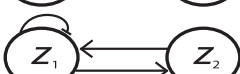
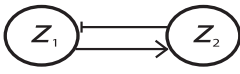
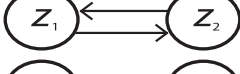
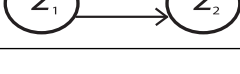
The case of autorepression also gives the possibility of two stable solutions in the case when the cross regulation defined as  $w_{12}$  and  $w_{21}$  is of the same type of coupling (that is, the cross regulation connections are both repressors or both activators). Changing the sign of a cross-regulation term in the 2-node system, graphically, results in a reflection of the nullcline about its central point. This reflection is a horizontal one if we consider a change in sign of  $w_{12}$  in the  $Z_1'$  equation and is a reflection about a vertical line for a change in sign of  $w_{21}$  in the  $Z_2'$  equation. In the cases when autorepression is the only type of auto-regulatory influence, less connections whether through no autoregulation ( $w_{ii} = 0$  for either  $i = 1$  or  $2$ ) or only one cross regulation ( $w_{12} = 0$  or  $w_{21} = 0$ ) has the effect of reducing the number of stable solutions to one. When there is a mixed auto-regulatory type of influence (e.g., autorepression-autoactivation) less connections via  $w_{ii}$  or  $w_{ij}$  becoming zero, does not necessarily result in a single stable solution. In this mixed auto-regulatory case the deletion of the autoactivation connection does not necessarily change the number of equilibria nor the corresponding solutions when the cross regulations are of the same type (and it can lead to only one stable solution when the cross regulations are mixed or when there is only one).

Reduction of connections in the case of autoactivation-autoactivation reduces the number of potential stable equilibrium solutions from 4 to 2 as long as one of the auto-regulatory connections remains. If both regulatory influences are deleted then this can lead to a single stable solution except in the case when cross regulations of the same type persist. The most influential regulatory interactions that lead to more than one stable equilibrium are the autoactivation and same type of cross regulation connections.

It is also common to have non-autoregulating genes that connect to each other. When this cross-connection is the same type of connection, we observe that we can actually have two stable equilibria. For example, if we take  $w_{ii} = 0$ ,  $w_{ij} = -3.3$ ,  $b_i = -8$ ,  $k_i = 7$ , and  $d_i = 1$ , we see that have three equilibria with two of them stable solutions; see [Fig. 3B](#). Otherwise, in the cases of non-autoregulating coupled genes with mixed type of cross regulation or a single cross regulation we have a single globally stable equilibrium solution.

**Table 1**

Possible total equilibria and the corresponding number of stable equilibrium solutions for the coupled 2-node system. In all cases, there will always be at least one stable equilibrium solution. Columns 1 and 2 specified the types of auto- and cross-regulatory interactions. Autoactivators satisfy  $w_{ii} > 0$ , autorepressors satisfy  $w_{ii} < 0$ , and no autoactivation corresponds to  $w_{ii} = 0$ . Cross-regulation is “single only” if  $w_{ij} = 0$  and  $w_{ji} \neq 0$ . If  $w_{ij}w_{ji} < 0$  cross-regulation is “mixed”, whereas if  $w_{ij}w_{ji} > 0$  cross-regulation is “same”. For “mixed” and “single only” cases the same results hold for cross-repression even though diagrams correspond to cross-activation.

Type of autoregulation	Type of cross regulation	Possible equilibria	Possible stable equil.	Example of connection
Autoactivate -	Mixed	9	4	
Autoactivate	Same	9	4	
	single only	9	4	
autoactivate -	mixed	5	2	
no autoregulation	same	3	2	
	single only	3	2	
autoactivate -	mixed	5	2	
autorepress	same	3	2	
	single only	3	2	
autorepress -	mixed	1	1	
autorepress	same	3	2	
	single only	1	1	
autorepress -	mixed	1	1	
no autoregulation	same	3	2	
	single only	1	1	
no autoregulation-	mixed	1	1	
no autoregulation	same	3	2	
	single only	1	1	

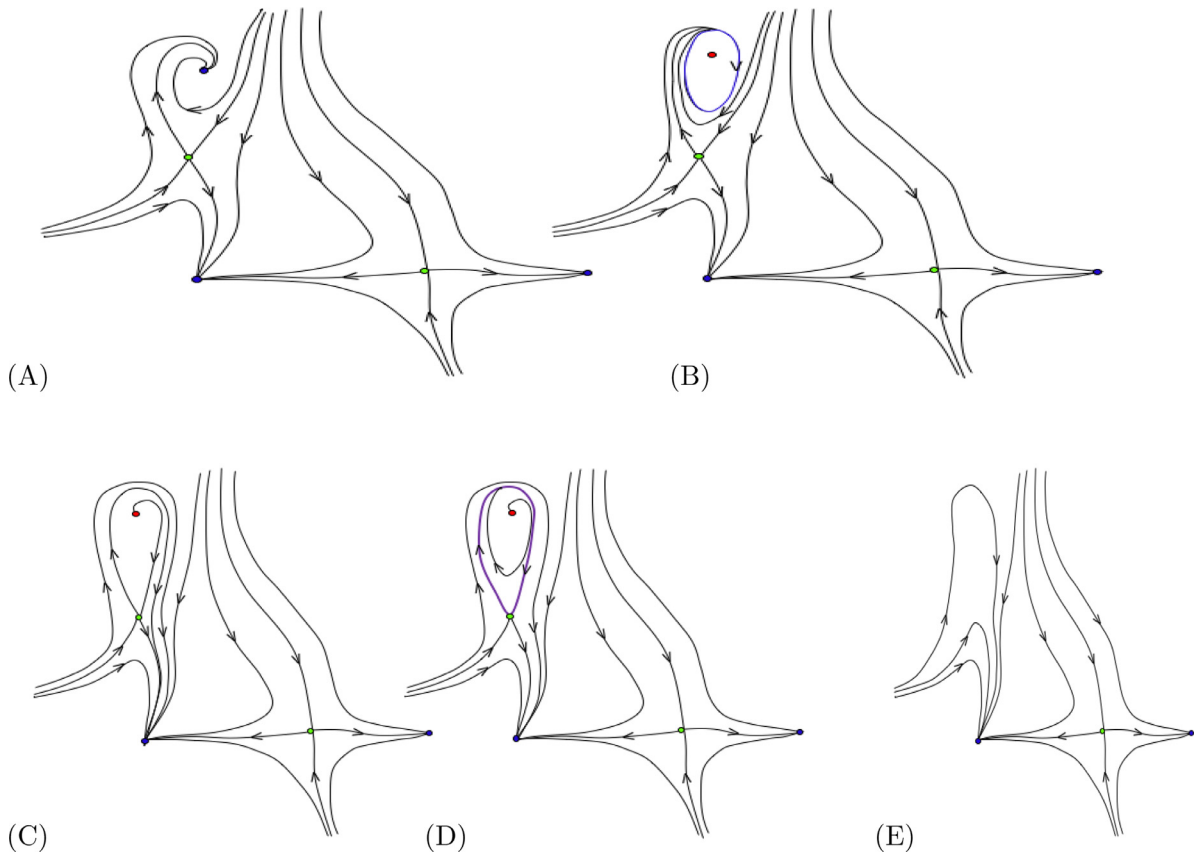


**Fig. 8.** Succession of phase plane diagrams focused on the region  $[-0.5, 1.5] \times [-0.5, 1.5]$ , as the system is undergoing the bifurcation sequence shown in Fig. 6D. The flow lines are shown as black curves, with arrows indicating the direction. (A): The system starts with three attracting equilibria (two stable nodes and one stable spiral, all shown as blue dots), and two saddles (both shown as green dots). (B): The system undergoes a supercritical Hopf bifurcation at  $w_{12} = 0.14052081$ , with loss of stability of the stable spiral (top left) and creation of an attracting cycle. (C): After increasing, the cycle undergoes a homoclinic bifurcation at  $w_{12} = 0.141386$  (C), and breaks (D). (E): Later, at  $w_{12} = 0.17164026$ , the newly formed unstable equilibrium collides with the left saddle and both disappear through a saddle node bifurcation. (For interpretation of the references to color in this figure legend, the reader is referred to the web version of this article.)

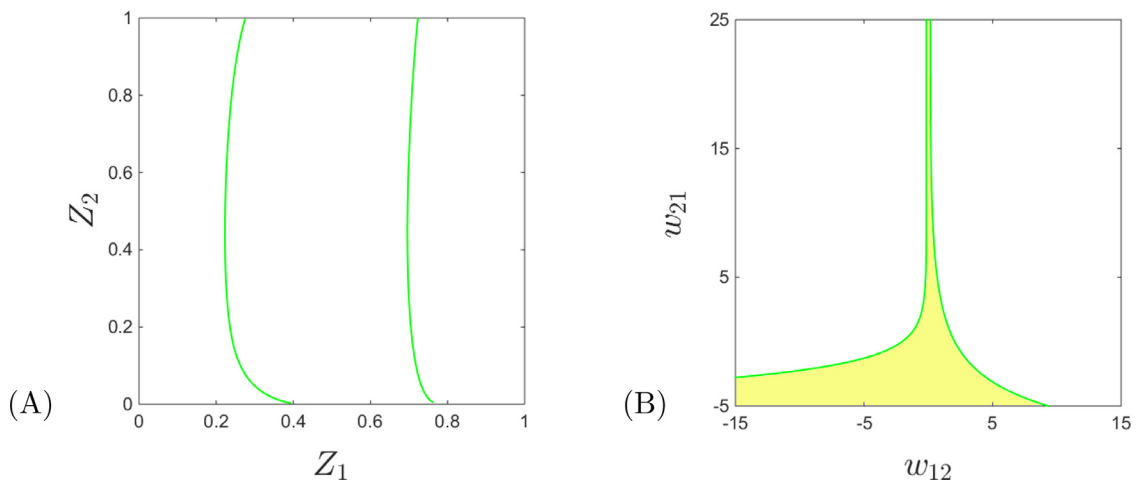


**Fig. 9.** Saddle Node curves with respect to  $w_{12}$  and  $w_{21}$ . (A): The  $(Z_1, Z_2)$  phase plane (left). (B): The  $(w_{12}, w_{21})$  parameter plane (right), for fixed  $w_{11} = 5$  and  $w_{22} = 0$ . The other parameters are fixed to  $d_1 = d_2 = 1$ ,  $k_1 = k_2 = 1$ ,  $b_1 = b_2 = 2.5$ . The system has a unique stable equilibrium outside the Saddle Node curves, and has three equilibria (two attracting and one saddle) in the shaded region between the Saddle Node curves.

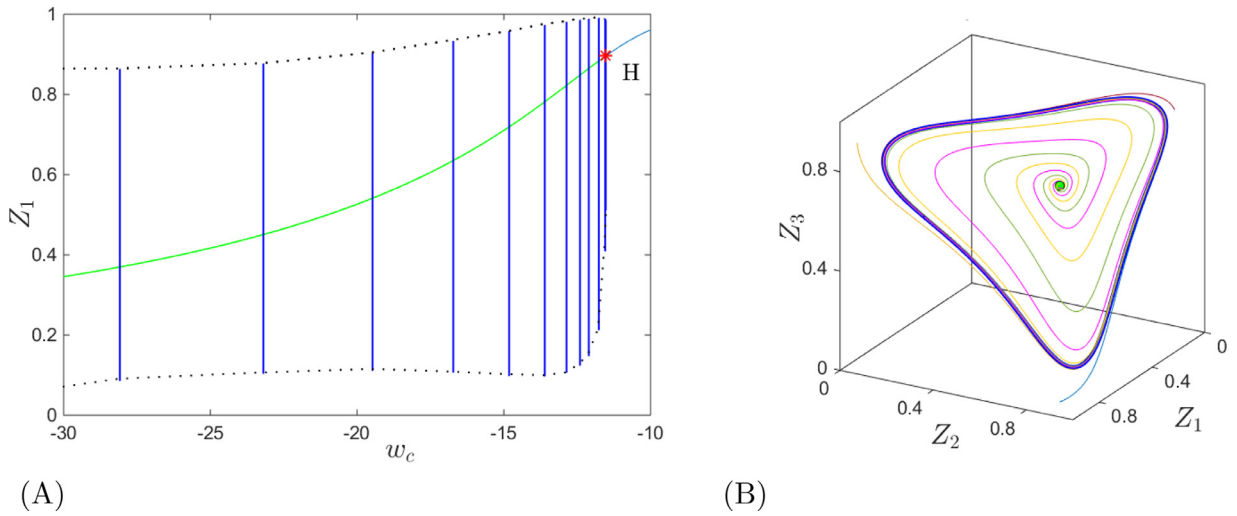


**Fig. 10.** Supercritical Hopf bifurcation in the 3D system with respect to  $w_c$ . Fixed parameters:  $k_1 = k_2 = k_3 = 1$ ,  $d_1 = d_2 = d_3 = 1$ ,  $b_1 = b_2 = b_3 = -8$ ,  $w_a = 5$ ,  $w_{cc} = 0$ . The Hopf bifurcation occurs at  $w_c = -11.519135$ , with Lyapunov coefficient  $\sigma = -1.1377$ . (A): Bifurcation diagram, showing the equilibrium curve and its transition into a cycle, represented as the  $Z_1$  projection against the key parameter  $w_c$ . The Hopf point (H) is shown as a red star, the equilibrium past the Hopf point is shown as a green curve, and a few instances of the cycle are illustrated (in their  $Z_1$  projection) as vertical blue lines. Dotted black curves track the evolution of the highest and lowest  $Z_1$  values of the cycle, as  $w_c$  evolves. (B): Phase space for  $w_c = -12$ , where the system has a cycle. The equilibrium (green dot) attracts only in the direction of the diagonal  $Z_1 = Z_2 = Z_3$ . All other initial conditions converge asymptotically towards the thick blue cycle (a few trajectories shown in thin line of different colors). (For interpretation of the references to color in this figure legend, the reader is referred to the web version of this article.)

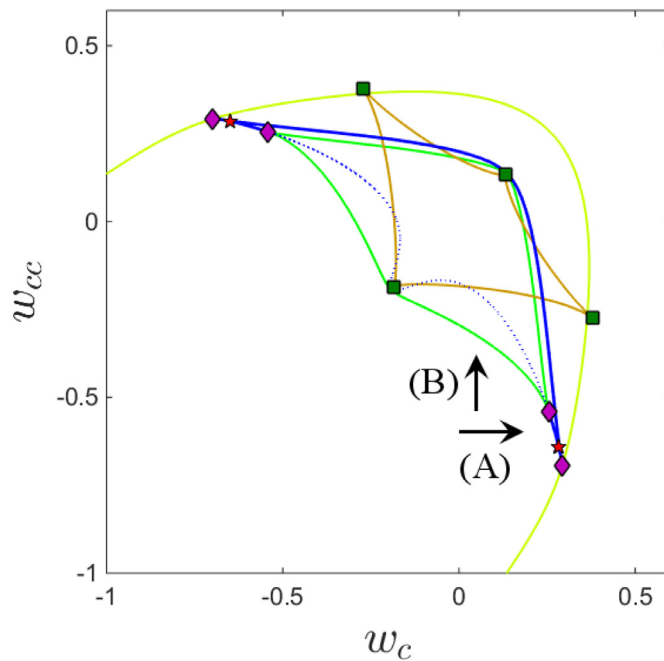


**Fig. 11.** Examples of bifurcations in the 3-dimensional system, with respect to the strength ( $w_c$ ,  $w_{cc}$ ). Fixed parameters:  $k_1 = k_2 = k_3 = 1$ ,  $d_1 = d_2 = d_3 = 1$ ,  $b_1 = b_2 = b_3 = 2.5$ ,  $w_a = 5$ . Top panel shows a few bifurcation curves in the region  $[-1, 0.5] \times [-1, 0.5]$  of the parameter plane: Saddle Node curves are shown in different shades of green and yellow, and a Hopf curve is shown in blue. The relevant codimension two bifurcation points are marked along these curves: Cusp Points as green squares, Bogdanov-Takens points as purple diamonds, and the Generalized Hopf bifurcation (where the supercritical and subcritical Hopf branches meet) as a red star. The Neutral Saddle curve connecting the Hopf pieces (joining them at the Bogdanov-Takens points) is shown as a blue dotted line. Fig. 12 illustrates two examples of phase space transition sequences along paths in this parameter plane, one for fixed  $w_{cc}$  and variable  $w_c$  (indicated by the arrow marked (A), and illustrated in Fig. 12A), and one for fixed  $w_c$  and variable  $w_{cc}$  (indicated by the arrow marked (B) and illustrated in Fig. 12B). (For interpretation of the references to color in this figure legend, the reader is referred to the web version of this article.)

3.2. Other stable modes in 2-node model

Besides multistability, other stable modes such as a stable limit cycle may be present in an observed gene profile. To examine other stable modes, we observe that an equilibrium  $(Z_1^*, Z_2^*)$  satisfies  $k_1 S_1 = d_1 Z_1^*$  and  $k_2 S_2 = d_2 Z_2^*$ , where we called

$$S_1 = \frac{1}{1 + \exp(-w_{11}Z_1^* - w_{12}Z_2^* + b_1)} \text{ and } S_2 = \frac{1}{1 + \exp(-w_{21}Z_1^* - w_{22}Z_2^* + b_2)}.$$

We calculate the Jacobian of the system at an equilibrium  $(Z_1^*, Z_2^*)$  (and drop the \* for legibility):

$$J(Z_1^*, Z_2^*) = \begin{pmatrix} k_1 w_{11}(S_1 - S_1^2) - d_1 & k_1 w_{12}(S_1 - S_1^2) \\ k_2 w_{21}(S_2 - S_2^2) & k_2 w_{22}(S_2 - S_2^2) - d_2 \end{pmatrix}$$

$$= \begin{pmatrix} k_1 w_{11} \left( \frac{d_1 Z_1}{k_1} - \frac{d_1^2 Z_1^2}{k_1^2} \right) - d_1 & k_1 w_{12} \left( \frac{d_1 Z_1}{k_1} - \frac{d_1^2 Z_1^2}{k_1^2} \right) \\ k_2 w_{21} \left( \frac{d_2 Z_2}{k_2} - \frac{d_2^2 Z_2^2}{k_2^2} \right) & k_2 w_{22} \left( \frac{d_2 Z_2}{k_2} - \frac{d_2^2 Z_2^2}{k_2^2} \right) - d_2 \end{pmatrix}.$$

If we call  $\lambda_1$  and  $\lambda_2$  the eigenvalues of the matrix  $J(Z_1^*, Z_2^*)$ , then

$$\lambda_1 + \lambda_2 = \text{Tr}(J) = w_{11}k_1 \left( \frac{d_1 Z_1}{k_1} - \frac{d_1^2 Z_1^2}{k_1^2} \right) + w_{22}k_2 \left( \frac{d_2 Z_2}{k_2} - \frac{d_2^2 Z_2^2}{k_2^2} \right) - d_1 - d_2$$

$$= -w_{11}k_1 \left( \frac{d_1 Z_1}{k_1} - \frac{1}{2} \right)^2 - w_{22}k_2 \left( \frac{d_2 Z_2}{k_2} - \frac{1}{2} \right)^2 + \frac{w_{11}k_1}{4} + \frac{w_{22}k_2}{4} - d_1 - d_2.$$

Hence  $\text{Tr}(J) = 0$  for equilibria on the phase plane circle ellipse

$$k_1 w_{11} \left( \frac{d_1 Z_1}{k_1} - \frac{1}{2} \right)^2 + k_2 w_{22} \left( \frac{d_2 Z_2}{k_2} - \frac{1}{2} \right)^2 = \frac{w_{11}k_1}{4} + \frac{w_{22}k_2}{4} - d_1 - d_2.$$

In the following calculations, we let  $A = \frac{d_1 Z_1}{k_1} - \frac{d_1^2 Z_1^2}{k_1^2}$  and  $B = \frac{d_2 Z_2}{k_2} - \frac{d_2^2 Z_2^2}{k_2^2}$  for simplicity. Then we can express (calling the coupling determinant  $\Delta = w_{11}w_{22} - w_{12}w_{21}$ ):

$$\lambda_1 \lambda_2 = \det(J) = (k_1 w_{11}A - d_1)(k_2 w_{22}B - d_2) - k_1 k_2 w_{12} w_{21} AB$$

$$= k_1 k_2 \Delta AB - k_1 w_{11} d_2 A - k_2 w_{22} d_1 B + d_1 d_2.$$

If we assumed that  $\text{Tr}(J) = k_1 w_{11}A + k_2 w_{22}B - d_1 - d_2 = 0$ , one can substitute  $B$  into the expression of the determinant and get (where  $\Delta = w_{11}w_{22} - w_{12}w_{21}$ ):

$$w_{22} \det(J) = k_1 \Delta A(d_1 + d_2 - k_1 w_{11}A) - k_1 d_2 w_{11} w_{22} A - d_1 w_{22}(d_1 + d_2 - k_1 w_{11}A) + w_{22} d_1 d_2$$

$$= -k_1^2 w_{11} \Delta A^2 + [k_1 \Delta(d_1 + d_2) + k_1 w_{11} w_{22}(d_1 - d_2)]A - d_1^2 w_{22}.$$

This is a quadratic expression in  $A$ , whose discriminant is

$$D = [k_1 \Delta(d_1 + d_2) + k_1 w_{11} w_{22}(d_1 - d_2)]^2 - 4k_1^2 d_1^2 \Delta w_{11} w_{22}$$

$$= k_1^2 [\Delta^2(d_1 + d_2)^2 + w_{11}^2 w_{22}^2 (d_1 - d_2)^2 - 2\Delta w_{11} w_{22}(d_1 + d_2)^2 + 4\Delta w_{11} w_{22} d_1 d_2]$$

$$= k_1^2 [(d_1 + d_2)^2 (\Delta^2 - 2\Delta w_{11}^2 w_{22}^2 + w_{11}^2 w_{22}^2) - 4w_{11}^2 w_{22}^2 d_1 d_2 + 4\Delta w_{11} w_{22} d_1 d_2]$$

$$= k_1^2 [(d_1 + d_2)^2 (\Delta - w_{11} w_{22})^2 + 4w_{11}^2 w_{22}^2 d_1 d_2 (\Delta - w_{11} w_{22})]$$

$$= k_1^2 w_{12} w_{21} [(d_1 + d_2)^2 w_{12} w_{21} - 4d_1 d_2 w_{11} w_{22}]$$

If one considers the parameter subset  $w_{ij} > 0$ , we can notice that, if  $\frac{w_{11}w_{22}}{w_{12}w_{21}} - 1 > \frac{(d_1 - d_2)^2}{4d_1 d_2}$ , then  $(d_1 + d_2)^2 w_{12} w_{21} - 4d_1 d_2 w_{11} w_{22} < 0$  and so  $D < 0$ , implying that  $\det(J) < 0$  and hence a Jacobian with two real distinct eigenvalues of opposite sign (neutral saddle) every time  $\text{Tr}(J) = 0$ . The existence of a Hopf bifurcation is therefore impossible for the system operating in this regime, which occurs in particular, for example, in the symmetric case  $d_1 = d_2$ , if  $w_{11}w_{22} > w_{12}w_{21}$  (i.e., if the nodes' autoregulation is higher than the cross-regulation). However, under different circumstances, both subcritical and supercritical Hopf bifurcations may occur, introducing transitions of stable/unstable equilibria into stable/unstable limit cycles. We keep this in mind below, where we analyze some cases of interest for the system parameters.

Case  $w_{11} = w_{22} > 0$

In this case, both nodes are autoactivating and we consider first the symmetric case for their respective strengths and decay rates and assume that both are repressors.

Fig. 4 illustrates the bifurcation diagram of the system with respect to the cross-node weights ( $w_{12}, w_{21}$ ) in the region  $0 \leq w_{12}, w_{21} \leq 1$ , in the case  $d_1 = d_2 = 1$ ,  $w_{11} = w_{22} = 5$ , for  $b_1 = b_2 = 2.5$  and  $k_1 = k_2 = 1$ . The bifurcation curves are shown in both the variable  $(Z_1, Z_2)$  plane (Fig. 4A), as well as in the parameter  $(w_{12}, w_{21})$  plane (Fig. 4B). There are no Hopf bifurcations, but rather an ellipse of neutral saddles, which in this case is the circle

$$\left(Z_1^2 - \frac{1}{2}\right) + \left(Z_2^2 - \frac{1}{2}\right) = \frac{1}{10}$$

shown as a thin dotted curve in both panels (since crossing a neutral saddle curve does not affect the number or stability of equilibria). Saddle node curves are shown in corresponding shades of green and yellow between the two panels, with Cusp Points (i.e., points where two Saddle Node branches meet tangentially) marked as green squares. Fig. 5 illustrates, for the same fixed parameters, the evolution of the equilibrium curves for the system in the plane  $(Z_1, Z_2)$ , along the slice  $w_{12} = w_{21}$ .

The top panels of Fig. 6 illustrate the same bifurcation diagrams of the system with asymmetric  $d_1 = 1$  and  $d_2 = 0.75$ , and the other fixed parameters the same as before:  $w_{11} = w_{22} = 5$ ,  $b_1 = b_2 = 2.5$ ,  $k_1 = k_2 = 1$ . In this scenario, zero sum eigenvalues may produce a Neutral Saddle, if the eigenvalues are real (which we again illustrate as a thin dotted curve), but also allows for Hopf bifurcations, when the transition happens with  $\det(J) > 0$  and the eigenvalues are complex. In the latter case, these portions of the curve in Fig. 6 are illustrated as a thick blue line. The Hopf curves terminate at Bogdanov-Takens codimension two bifurcation points (shown as purple squares), which are intersections of the Hopf curve with two Saddle Node branches and a Homoclinic curve. (Beyond the Hopf curve portions, these Bogdanov-Takens points are further connected by the Neutral Saddle curve.) The Homoclinic curves are not shown in the parameter plane in Fig. 6B, since it was difficult to lower the step size enough to extend the numerical algorithm along each curve. Instead, we illustrate in Fig. 6C–E three examples of Hopf bifurcations at different points on the Hopf segments; we show how the cycle is formed as the blue curve is crossed, and how the cycle disappears via a saddle homoclinic bifurcation, as the Homoclinic curve is crossed. All three Hopf bifurcations (subcritical and supercritical) are obtained by varying  $w_{12}$  when  $w_{21}$  is fixed.

Fig. 6C illustrates an example of a subcritical Hopf bifurcation with respect to  $w_{12}$ , for fixed  $w_{21} = -6$  (i.e., when crossing the lower Hopf curve below the red star). For small positive  $w_{12}$  ( $= 0.1$ ) and  $w_{21} = -6$ , the system has a locally stable equilibrium at  $(Z_1, Z_2) = (0.2067545174, 1.216268606)$ . When extending with respect to  $w_{12}$ , the equilibrium runs into a subcritical Hopf bifurcation at  $w_{12} = 0.14037185$ , with  $(Z_1, Z_2) = (0.23995684, 1.0493532)$ , and Lyapunov coefficient  $\sigma = 3.778149 > 0$ . We further run into a nearby saddle node at  $w_{12} = 0.14472012$ , with  $(Z_1, Z_2) = (0.22709203, 0.96555485)$ . Note that there are other bifurcation points on the curve, not shown in our range. The unstable cycle born at the Hopf point extends with respect to  $w_{12}$  as its period increases, until  $w_{12} \sim 0.13948166$ , where it runs into the other branch of the equilibrium point born at the saddle node, and disintegrates (as shown in Fig. 6B).

Fig. 6D illustrates an example of a supercritical Hopf bifurcation with respect to  $w_{12}$ , for fixed  $w_{21} = -5$  (i.e., when crossing the lower Hopf curve above the red star). For  $w_{12} = 0$  and  $w_{21} = -5$ , the system has three stable equilibria and two unstable (saddles). While the stability of the other three equilibria is robust with respect to changes in  $(w_{12}, w_{21})$ , the remaining stable/unstable pair undergoes bifurcations. The figure shows how this locally stable equilibrium, originally at  $(Z_1, Z_2) = (0.14479411, 1.2798605)$ , extends as  $w_{12}$  increases, and undergoes a supercritical Hopf point at  $w_{12} = 0.14052081$ , with  $(Z_1, Z_2) = (0.28986285, 1.100445)$  and Lyapunov coefficient  $\sigma = -3.843708 < 0$ . The locally stable cycle born from the Hopf bifurcation survives until  $w_{12} = 0.141386$ , where it is destroyed via a homoclinic bifurcation, as it collides with the saddle branch of the equilibrium point. The unstable equilibrium born of the Hopf bifurcation is later destroyed at  $w_{12} = 0.17164026$  (with  $(Z_1, Z_2) = (0.23924595, 0.85616415)$ ), where it collides with the saddle via a saddle-node bifurcation. Since this is the biologically interesting case revealing that the system can have stable oscillations, we illustrate in more detail the phase plane transitions of the system. To clarify the numerically-generated phase planes shown in Fig. 7, we created hand-drawn sketches of the phase plane in Fig. 8, which more clearly illustrate the phase transitions at the bifurcation points, and the asymptotic dynamics in the intervals between them.

Fig. 6E illustrates an example of a supercritical Hopf bifurcation with respect to  $w_{12}$ , for fixed  $w_{21} = -5$  (i.e., when crossing the higher Hopf curve). For  $w_{12} = 0.5$  and  $w_{21} = -1$ , the system has a locally stable equilibrium at  $(Z_1, Z_2) = (0.22023529, 0.26889983)$ . As  $w_{12}$  is decreased, the equilibrium changes stability at  $w_{12} = 0.4869$  via a supercritical bifurcation, with  $(Z_1, Z_2) = (0.232371, 0.293394)$  and Lyapunov coefficient  $\sigma = -9.088$ . The stable cycle formed through this bifurcation increases in amplitude as  $w_{12}$  further decreases, and disappears at  $w_{12} \sim 0.4864$  via a homoclinic saddle collision with another equilibrium branch.

Case  $w_{11} > 0$  and  $w_{22} = 0$

In this case, one node is an autoactivator while the other is not an autoregulator. The condition for  $\text{Tr}(J) = 0$  in this case translates to  $k_1 \left( \frac{d_1 Z_1}{k_1} - \frac{1}{2} \right)^2 = \frac{w_{11} k_1}{4} - d_1 - d_2$ . This does not happen generically for the system at equilibrium, hence there will be Hopf or neutral saddle points. This is the case in Fig. 9, which suggests that, in particular, there are only saddle node bifurcations with respect to  $w_{12}$  and  $w_{21}$ , for the same fixed symmetric parameters as before.

Case  $w_{21} = w_{22} = 0$ , and  $w_{11} \leq 0$ .

In this case, one node is an autorepressor while the other is not an autoregulator and we allow for only a one-way connection between the two nodes. In this case, the second equation becomes  $\frac{dZ_2}{dt} = \frac{k_2}{1 + e^{b_2}} - d_2 Z_2$ , hence the second component of the equilibrium is  $Z_2^* = \frac{k_2}{d_2(1 + e^{b_2})}$ . If  $w_{11} = 0$  (no autoregulation), then the first equation is  $\frac{dZ_1}{dt} = \frac{k_1}{1 + \exp(-w_{12}Z_2 + b_1)} - d_1 Z_1$  and the first component of the equilibrium is  $Z_1^* = \frac{k_1}{d_1(1 + \exp(-w_{12}Z_2^* + b_1))}$ , hence the system has a unique equilibrium. In addition, the Jacobian at this equilibrium is the upper triangular matrix

$$J(Z_1^*, Z_2^*) = \begin{pmatrix} -d_1 & \frac{k_1 w_{12} \exp(-w_{12}Z_2^* + b_1)}{[1 + \exp(-w_{12}Z_2^* + b_1)]^2} \\ 0 & -d_2 \end{pmatrix},$$

with negative eigenvalues  $-d_1$  and  $-d_2$ , hence the equilibrium is always stable. This remains the case if  $w_{11} < 0$ . In this case the first component of the equilibrium is given by

$$\frac{dZ_1}{dt} = \frac{k_1}{1 + \exp(-w_{11}Z_1 - w_{12}Z_2^* + b_1)} - d_1 Z_1 = 0.$$

Since  $w_{11} < 0$ , the left hand side is a strictly decreasing, continuous function, which is negative for  $Z_1 \rightarrow \infty$  and positive for  $Z_1 \rightarrow -\infty$ , hence it equals zero at one unique point  $Z_1 = Z_1^*$ . The system again has a unique equilibrium, with upper triangular Jacobian matrix:

$$J(Z_1^*, Z_2^*) = \begin{pmatrix} -d_1 + \frac{k_1 w_{11} \exp(-w_{11}Z_1^* - w_{12}Z_2^* + b_1)}{[1 + \exp(-w_{11}Z_1^* - w_{12}Z_2^* + b_1)]^2} & * \\ 0 & -d_2 \end{pmatrix}.$$

Since  $d_1, d_2, k_1 > 0$  and  $w_{11} < 0$ , both eigenvalues (diagonal entries) are negative, and the system has again a unique attracting node.

### 3.3. Three-dimensional model

We briefly consider the case of three nodes:

$$\frac{dZ_1}{dt} = \frac{k_1}{1 + \exp(-w_{11}Z_1 - w_{12}Z_2 - w_{13}Z_3 + b_1)} - d_1 Z_1 \tag{9}$$

$$\frac{dZ_2}{dt} = \frac{k_2}{1 + \exp(-w_{21}Z_1 - w_{22}Z_2 - w_{23}Z_3 + b_2)} - d_2 Z_2 \tag{10}$$

$$\frac{dZ_3}{dt} = \frac{k_3}{1 + \exp(-w_{31}Z_1 - w_{32}Z_2 - w_{33}Z_3 + b_3)} - d_3 Z_3 \tag{11}$$

**Result 3:** Consider the 3-node system (9)–(11):  $Z_1' = f_1$ ,  $Z_2' = f_2$ , and  $Z_3' = f_3$  with  $w_{ii} > 0$  for  $i = 1, 2, 3$  (three autoactivators) and  $0 < Z_i < \frac{k_i}{d_i}$ . For any  $k_i, d_i > 0$ , there exists  $b_i$  and  $w_{ij}$  with  $i \neq j$  ( $i, j = 1, 2, 3$ ) such that 27 equilibrium solutions exist. Moreover, eight of these equilibrium solutions are stable.

The proof in both the uncoupled and coupled scenarios are similar to Result 2. The uncoupled case is completely analogous. For the coupled case, for small  $w_{ij}$  and bounded  $Z_j$  we have that  $\exp(\sum_j -w_{ij}Z_j) \approx C \approx 1$  and thus the remainder of the argument holds just like in Result 2. However, as with the case of two nodes, we see that the  $w_{ij}$  do not need to be small in order for the result to hold. For example, choosing three symmetric regulatory connections with  $k_i = 7$ ,  $d_i = 1$ ,  $b_i = 15$ ,  $w_{ii} = 3$  all for  $i = 1, 2, 3$ , and  $w_{ij} = 1$  (for  $i \neq j$ ) will give the number and stability of the equilibrium solutions stated in Result 3.

As one could build the subnetwork from two genes to three and eventually to the full number, we want to know what may happen when we add additional genes—whether this will allow for more possible equilibria, keep the number the same, or reduce the number of equilibria that are possible. Graphically, by examining the surface defined by  $Z_i' = 0$  for  $i = 1, 2$ , or 3 we see that including an additional plane or surface to the 2-node system will at least keep the number and stability of the equilibria given in Table 1. For example, if we consider the autoactivator-autoactivator pair coupled together with a non-autoregulating node, we can still have up to four stable equilibria. If we compare to Fig. 1, we see that this type of situation would apply to any gene connected to the RAP1-RCS1 pair. We may, in certain situations end up with additional equilibria by including an extra connection. For example, if we consider three non-autoregulating nodes that are cross-connected in the same way with  $w_{ii} = 0$ ,  $b_i = -8$ ,  $k_i = 7$ ,  $d_i = 1$  all for  $i = 1, 2, 3$ , and  $w_{ij} = -3.3$  (for  $i \neq j$ ) then we will have seven equilibria with three of them stable. While this specific 3-node combination is not seen in Fig. 1, we could imagine that it could occur in other systems.

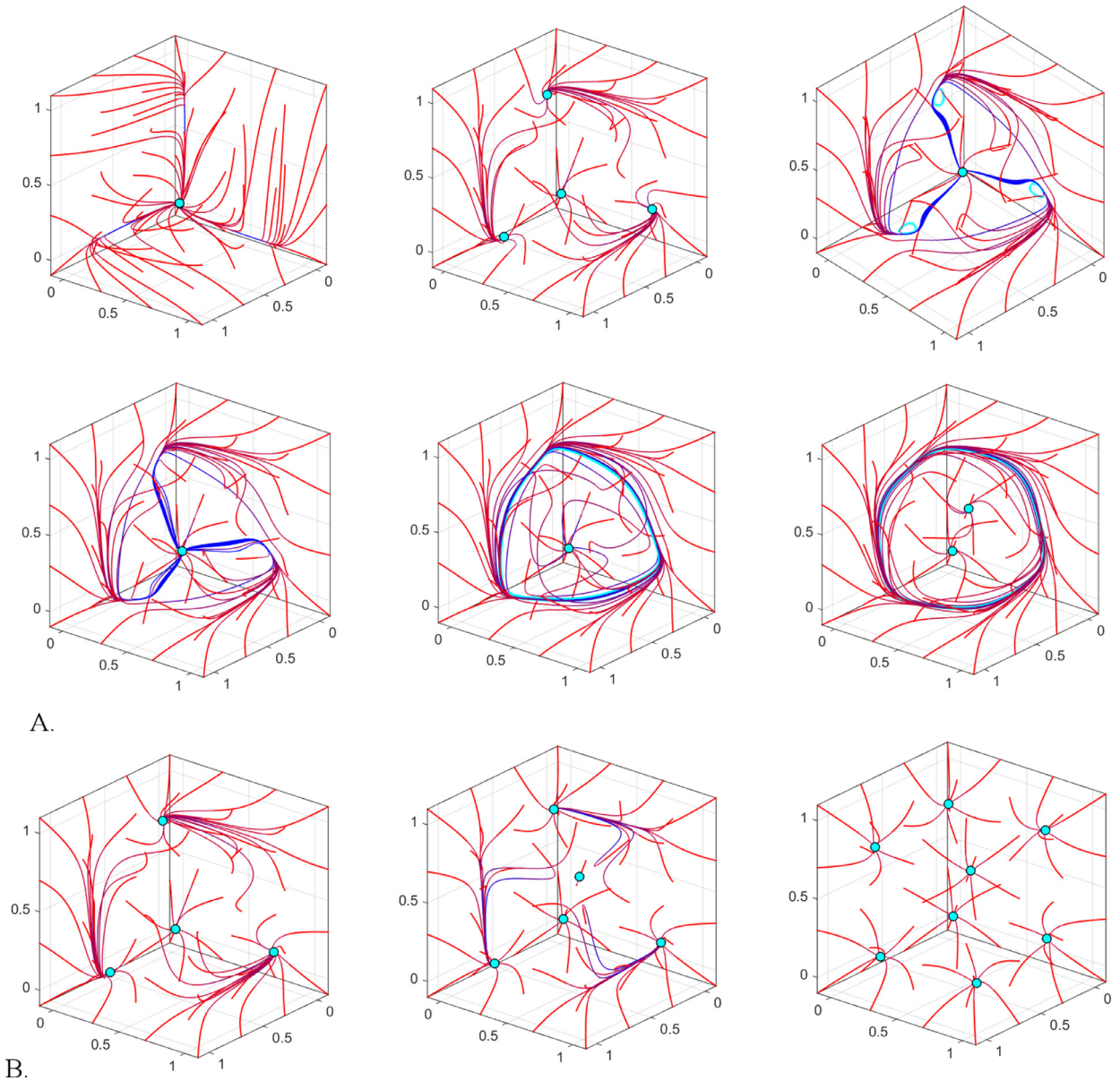


**Fig. 12.** Two examples of phase space transition sequences along paths in the parameter plane in Fig. 11: one for fixed  $w_{cc}$  and variable  $w_c$ , and one for fixed  $w_c$  and variable  $w_{cc}$  (as indicated by the black arrows marked (A) and (B) in Fig. 11). In all panels, trajectories are shown for a 3-dimensional grid of initial conditions with resolution 0.4, color coded to evolve in time from red to blue. Only stable equilibria are shown (in cyan). Limit cycles with attraction basins of dimension two are also shown in cyan. To better illustrate the symmetry in the system, we chose an angular view of the 3D phase-space close to the diagonal  $Z_1 = Z_2 = Z_3$  (with a small tilt, so as to not obstruct our view of the transitions which actually occur on the diagonal). (A) For fixed  $w_{cc} = -0.6$ , the panels show the phase spaces for  $w_c = -2.6, 0.2, 0.2373, 0.25, 0.34, 0.5$  from left to right and top to bottom. (B) For fixed  $w_c = 0.1$ , the panels show the phase spaces for  $w_{cc} = -0.4, -0.3, -0.1$  from left to right. More details on the dynamic signature of each phase space and on the transitions between them are discussed in the main text. (For interpretation of the references to color in this figure legend, the reader is referred to the web version of this article.)

3.4. Other stable modes in 3-node model

In order to simplify our search for specific behaviors (e.g., multistability and oscillations), we consider a reduced model, with fewer parameters: all nodes have identical auto-regulation  $w_a$ , are connected identically to their clockwise neighbors:  $w_{21} = w_{32} = w_{13} = w_c$  and to their counter-clockwise neighbors:  $w_{12} = w_{23} = w_{31} = w_{cc}$ .

$$\frac{dZ_1}{dt} = \frac{k_1}{1 + \exp(-w_a Z_1 - w_{cc} Z_2 - w_c Z_3 + b_1)} - d_1 Z_1 \tag{12}$$

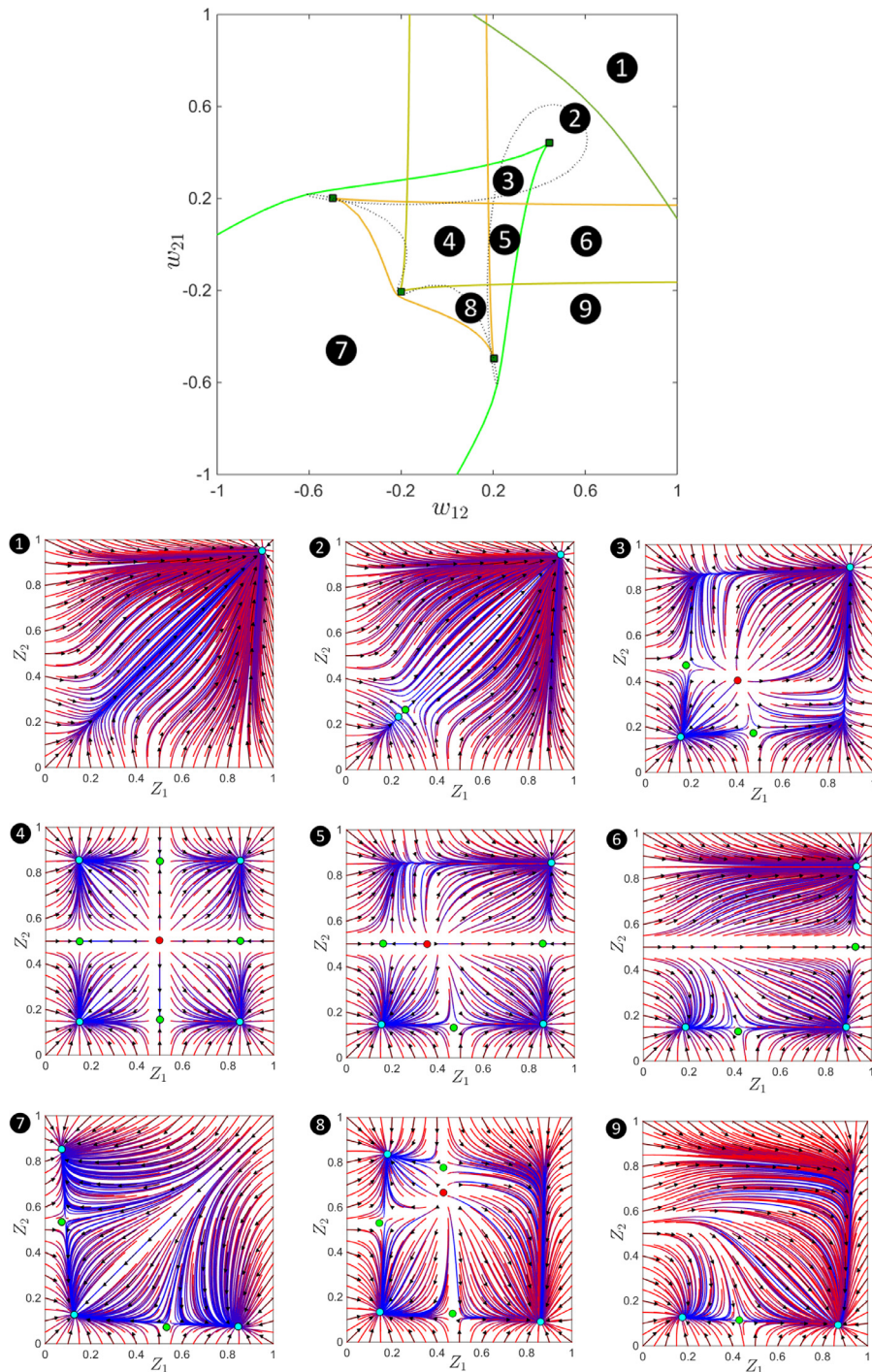


**Fig. 13.** Phase plane diagrams corresponding to different regions of Fig. 4. Nine pairs  $(w_{12}, w_{21})$  were chosen to illustrate the different stability regions of the parameter plane region  $[-1, 1] \times [-1, 1]$ . These regions were labeled (1)–(9) on the top bifurcation diagram (which reproduces identically Fig. 4B). Samples parameter points were chosen from each region as follows: (1)  $w_{12} = w_{21} = 0.8$ ; (2)  $w_{12} = w_{21} = 0.6$ ; (3)  $w_{12} = 0.2, w_{21} = 0.2$ ; (4)  $w_{12} = 0, w_{21} = 0$ ; (5)  $w_{12} = 0.2, w_{21} = 0$ ; (6)  $w_{12} = 0.6, w_{21} = 0$ ; (7)  $w_{12} = -0.5, w_{21} = -0.5$ ; (8)  $w_{12} = 0.1, w_{21} = -0.3$ ; (9)  $w_{12} = 0.6, w_{21} = -0.3$ . For each parameter point, the corresponding phase plane diagram is represented below, with the vector field shown as black arrows, the temporal trajectories evolving in color from red to blue, and with equilibria shown as dots: red (repelling); cyan (attracting) and green (saddle). The other parameters were fixed to the same values as in Fig. 4. (For interpretation of the references to color in this figure legend, the reader is referred to the web version of this article.)

$$\frac{dZ_2}{dt} = \frac{k_2}{1 + \exp(-w_c Z_1 - w_a Z_2 - w_{cc} Z_3 + b_2)} - d_2 Z_2 \quad (13)$$

$$\frac{dZ_3}{dt} = \frac{k_3}{1 + \exp(-w_{cc} Z_1 - w_c Z_2 - w_a Z_3 + b_3)} - d_3 Z_3. \quad (14)$$

Keeping the level of auto-regulation constant  $w_a = 5$  and varying  $w_c$  and  $w_{cc}$ , we search for accessible behaviors and transitions between them. As before, we look for saddle node bifurcations – signaling the possible transitions between regimes with one or more local attractors, and for supercritical Hopf bifurcations – marking possible transitions between a stable steady state and a stable oscillation.

For negative levels of the external input  $b_1 = b_2 = b_3 = -8$  and fixed  $w_{cc} = 0$ , we found a supercritical Hopf bifurcation at  $w_c^* = -11.519135$ , separating two regimes. For values larger than the critical value  $w_c > w_c^*$ , the system has an attracting equilibrium, which at the Hopf bifurcation loses two of the attracting dimensions. After the bifurcation, for  $w_c < w_c^*$ , it is only attracting points along the diagonal  $Z_1 = Z_2 = Z_3$ , the rest of the initial conditions converging asymptotically to the cycle that is formed at the bifurcation (as shown in Fig. 10).

For positive levels of the external input  $b_1 = b_2 = b_3 = 2.5$ , we found multiple equilibria undergoing a more complex cascade of Saddle Nodes and Hopf bifurcations. In Fig. 11, we illustrate how bifurcation curves partition the region  $[-1, 0.5] \times [-1, 0.5]$  of the  $(w_c, w_{cc})$  parameter plane into subregions with distinct dynamics, so that when crossing a boundary bifurcation curve the system may transition from a regime of monostability to one of multistability, or conversely. Sequences of complex transitions involving changes in stability profiles can be obtained by increasing or decreasing only one parameter value (i.e., either  $w_c$  or  $w_{cc}$ ). In Fig. 12, we illustrate two such examples of transition sequences, one obtained by fixing  $w_{cc}$  and increasing  $w_c$ , and the other by fixing  $w_c$  and allowing  $w_{cc}$  to increase.

The first example, shown in Fig. 12A, and marked by the black arrow (A) in Fig. 11, aims to illustrate formation and destruction of stable limit cycles, and coexistence of locally stable equilibria and cycles. While keeping  $w_{cc} = -0.6$ , the panels represent increasing values of  $w_c$  ( $-2.6, 0.2, 0.2373, 0.25, 0.34, 0.5$ , respectively, from left to right and top to bottom), and show the succession of the prototypical phase space behavior in each subregion that is crossed. For  $w_c = -2.6$ , the phase space shows one stable equilibrium. Then when  $w_c = 0.2$  the system crosses the first Saddle Node curve (out of the view range), which results in three additional stable equilibria that appear simultaneously due to the system's symmetry. (This situation is illustrated in the second set of panels in Fig. 12B, for the parameter  $w_c = 0.2$ .) When  $w_c$  is further increased, the system crosses the left side of the blue (supercritical) Hopf curve. At this moment the nondiagonal equilibria lose two of the stability dimensions, and each gives birth to a limit cycle with an attraction basin of dimension two (shown in cyan in the next panel for  $w_c = 0.2373$ ). These three cycles are destroyed simultaneously via homoclinic bifurcations (the Homoclinic curve is now shown in the parameter plane), leading to the cycle-free phase space illustrated in the next panel (for  $w_c = 0.25$ ). The system later gains a large cycle with a two-dimensional attraction basin (illustrated in cyan for  $w_c = 0.35$  in the next panel). More precisely, in this phase space all diagonal initial conditions are attracted by the diagonal equilibrium point, and the cycle attracts all other local initial conditions. The cycle appears via a fold bifurcation of cycles, in which the other, repelling cycle of the fold is generated when crossing the right branch of the blue (subcritical) Hopf curve. (The Fold bifurcation curve itself is not shown in the parameter plane.) Finally, the right Saddle Node curve is crossed, and a second attracting equilibrium appears on the diagonal (its unstable counterpart is not marked), as illustrated in the last panel (for  $w_c = 0.5$ ). The large attracting cycle later disappears, also via a Fold bifurcation (not shown in the Figure).

The second example, shown in Fig. 12B, and marked by the black arrow (B) in Fig. 11, illustrates successive formation of new stable equilibria via saddle node bifurcations, leading to high multistability in the central parameter subregion around the origin. For this experiment, the clockwise parameter was kept fixed to  $w_c = 0.1$ , and  $w_{cc}$  was successively increased. Increasing from  $w_{cc} = -0.4$  (left panel) to  $w_{cc} = -0.3$  (middle panel) crosses the lower Saddle Node bifurcation curve, resulting in gaining one additional stable equilibrium along the diagonal of the phase space. The corresponding unstable equilibrium born via this saddle node bifurcation is not marked. If the parameter is further increased to  $w_{cc} = -0.1$ , a second Saddle Node curve is crossed, giving birth by symmetry to six new equilibria simultaneously (three of them stable), for a total of eight locally stable equilibria within this parameter subregion.

The presence of additional stable modes may have implications for observed gene profiles.

#### 4. Discussion and conclusions

RNNs have often been used because of their robust numerical properties [34]. Previous work of Blasi et al. considered the symmetric case without external input for 2 nodes and 3 nodes [3]. Our results extend this and suggest that autoregulation is not as crucial in order to have multiple stable equilibria or modes. Using bifurcation analysis we have shown the existence of many other stable modes depending on parameter values. Knowing the multistable states in the  $n + 1$  vs.  $n$  node system is useful in trying to predict the effects of a knockout gene experiment *a priori*.

Additionally, our results suggest a reason why parameter values in the inferred gene networks in the literature may not always be realistic. Although the single connections may be fairly accurate (for inferring the network), the results here suggest that the parameter values play a crucial role and need to be addressed in such network-inferring models/algorithms (simply choosing more initial conditions is likely not sufficient). The results here also give insight into what can potentially

go wrong when using RNN models to infer the gene regulatory network through optimization code: (1) the routine may be assuming that there exists only one stable solution or (2) the minimum (which will yield the parameter values) may be in a basin of attraction of another stable solution (not the one consistent with the data) or near a stable manifold of a saddle solution and thus sensitive to initial conditions.

While experimental data is available for the maximal expression rates and degradation rates of the genes in our network, it is important to realize that the results presented here, in some sense, do not depend on these values. It is the case that if the  $k_i$  and  $d_i$  were to change then a different set of weights ( $w_{ij}$ ) and external inputs ( $b_i$ ) would be required to have the potential of multiple stable solutions. However, the importance of the Results is that we will always be able to find such  $w_{ij}$  and  $b_i$ . While the Results were shown for small values of cross-regulation, numerical evidence suggests that the Results hold for large values of the weights in many cases. Given that these parameters are often found through optimization, further investigation would be necessary to determine the consequences of a given choice of parameters. The fact that the steady state solutions remain bounded between 0 and  $k_i/d_i$  may help in understanding the above issues. Having other stable modes may also help further the understanding of what can potentially go wrong when using RNN models to infer the gene regulatory networks.

The role of autoregulation is also important in generating multistability, which is interpreted as a decision switch. Although bistability, interpreted as a progression switch, can likewise be generated with autoregulation, it was shown that both autorepression or no autoregulation can yield bistability as long as a sigmoidal behavior is present. In our particular subnetwork, Fig. 1 shows that there are five autoregulators within the network: YAP6, RAP1, RCS1, and SKN7 are autoactivators while SOK2 is the lone autorepressor. RAP1 and RCS1 thus have 4 potential stable solutions that they may attain depending on their parameters. While RCS1 is only connected to RAP1, we see that RAP1 is connected to three other nodes and thus knowing the possible stable solutions may be critical in determining the most accurate set of parameter values. SKN7 is autoactivated and connected with a single connection to two other nodes and this allows for 2 possible stable solutions. YAP6 is autoactivated and is highly connected. With each pair of nodes, we may have two possible stable solutions. Thus having 2 (or more) possible stable solutions may affect the outcome of the system or the values of other weights within the RNN.

Data from Lubeck shows that SOK2 is likely to have multiple steady states from its interaction with CRZ1 [25]. Some of the literature has also suggested that SOK2 activates CRZ1 and thus the bistability of SOK2 would be predicted by our Results [37]; however, even if this connection turns out to not be present, the subnetwork given in Fig. 1 places SOK2 within 1 connection of the potentially bistable YAP6-CUP9 connection and within 2 connections of the potentially multistable RCS1-RAP1-MSN4 connection. While CRZ1 is the initiator in the subnetwork presented here, it is clear that a better understanding of the nodes and their connectedness of this system is necessary for a complete understanding of the presence of multistability in the system.

## Acknowledgment

The authors would like to thank the reviewer for their thoughtful comments for improving the readability and presentation of the paper.

## Appendix A

In Fig. 13, we reproduce the bifurcation diagram in Fig. 4B, with more detail on the number of equilibria, their collisions and changes in stability when crossing the Saddle Node bifurcation curves from one region into another. While the symmetry and topological details of trajectories may differ within each region, representing a sample phase plane for each helps identify the regions with mono versus multi-stability, and the transitions between such regimes.

One can notice that crossing one Saddle Node branch comes with the birth/annihilation of a pair of equilibria, while crossing at the codimension-two points where these branching meet results in more complex transitions. For example, crossing from a point in region (3) into region (5) by decreasing  $w_{21}$  only, creates one new pair of stable/saddle equilibria, and the same happens when crossing into the region symmetric to (5) by decreasing  $w_{12}$  only. However, crossing via the codimension-two point directly into region (4) (by lowering  $w_{12}$  and  $w_{21}$  at the same time) produces simultaneously two stable - saddle equilibrium pairs. Similarly, when crossing from a point in region (3) into region (2) by increasing only  $w_{12}$  destroys one new pair of repelling/saddle equilibria, while crossing into region (5) by decreasing only  $w_{21}$  creates one pair of stable/saddle equilibria. However, changing  $w_{12}$  and  $w_{21}$  at the same time may lead to crossing into region (4) via the codimension-two point directly, which combines the two effects.

## References

- [1] Appgar JF, Witmer DK, White FM, Tidor B. Sloppy models, parameter uncertainty, and the role of experimental design. *Mol Biosyst* 2010;6:1890–900.
- [2] Bandyopadhyay S, et al. Rewiring of genetic networks in response to dna damage. *Science* 2010;330:1385–9.
- [3] Blasi MF, Casorelli I, Colosimo A, Blasi FS, Bignami M, Giuliana A. A recursive network approach can identify constitutive regulatory circuits in gene expression data. *Physica A* 2005;348:349–70.
- [4] Casey FP, Baird D, Feng Q, Gutenkunst RN, Waterfall JJ, Myers CR, et al. Optimal experimental design in an epidermal growth factor receptor signalling and down-regulation model. *IET Syst Biol* 2007;1(3):190–202.

- [5] Chou I, Voit EO. Recent developments in parameter estimation and structure identification of biochemical and genomic systems. *Math Biosci* 2009;219:57–83.
- [6] Dhooge A, Govaerts W, Kuznetsov YA, Mestrom W, Riet A, Sautois B. *Matcont and cl matcont: continuation toolboxes in matlab*. The Netherlands: Universiteit Gent, Belgium and Utrecht University; 2006.
- [7] Dhooge A, Govaerts W, Kuznetsov YA. *Matcont: a Matlab package for numerical bifurcation analysis of odes*. *ACM Trans Math Softw (TOMS)* 2003;29(2):141–64.
- [8] Engl HW, Flamm C, Kügler P, Lu J, Müller S, Schuster P. Inverse problems in system biology. *Inverse Probl* 2009;25:123014.
- [9] Garcia-Martinez J, Aranda A, Pérez-Ortín JE. Genomic run-on evaluates transcription rates for all yeast genes and identifies gene regulatory mechanisms. *Mol Cell* 2004;15(2):303–13.
- [10] Gardner T, Cantor C, Collins J. Construction of a genetic toggle switch in *escherichia coli*. *Nature* 2000;403:339–42.
- [11] Grigull J, Mnaimneh S, Pootoolal J, Robinson MD, Hughes TR. Genome-wide analysis of mrna stability using transcription inhibitors and microarrays reveals posttranscriptional control of ribosome biogenesis factors. *Mol Cell Biol* 2004;24(12):5534–47.
- [12] Guantes R, Poyatos JF. Multistable decision switches for flexible control of epigenetic differentiation. *PLoS Comput Biol* 2008;4:e1000235.
- [13] Gutenkunst RN, Waterfall JJ, Casey FP, Brown KS, Myers CR, Sethna JP. Universally sloppy parameter sensitivities in systems biology models. *PLoS Comput Biol* 2007;3:e189.
- [14] Holstege FC, Jennings EG, Wyrick JJ, Lee TI, Hengartner CJ, Green MR, et al. Dissecting the regulatory circuitry of a eukaryotic genome. *Cell* 1998;95(5):717–28.
- [15] Ingram PJ, Stumpf MP, Stark J. Network motifs: structure does not determine function. *BMC Genom* 2006;7:108.
- [16] Jeong J, Berman P. On cycles in the transcription network of *saccharomyces cerevisiae*. *BMC Syst Biol* 2008;2:12.
- [17] Kikuchi S, Tominaga D, Arita M, Takahashi K, Tomita M. Dynamic modeling of genetic networks using genetic algorithm and s-system. *Bioinformatics* 2003;19:643–50.
- [18] Kolda TG, Lewis RM, Torczon V. Optimization by direct search: new perspectives on some classical and modern methods. *SIAM Rev* 2003;45(3):385–482.
- [19] Lamb T, Mitchell A. The transcription factor rim101p governs ion tolerance and cell differentiation by direct repression of the regulatory genes *nrp1* and *smc1* in *saccharomyces cerevisiae*. *Mol Cell Biol* 2003;677–86.
- [20] Lee TI, Rinaldi NJ, Robert F, Odom DT, Bar-Joseph Z, Gerber GK, et al. Transcriptional regulatory networks in *saccharomyces cerevisiae*. *Science* 2002;298(5594):799–804.
- [21] Lee W-P, Tzou W-S. Computational methods for discovering gene networks from expression data. *Brief Bioinformatics* 2009;10:408–23.
- [22] Lee W-P, Yang K-C. Applying intelligent computing techniques to modeling biological networks from expression data. *Geno Prot Bioinfo* 2008;6:111–20.
- [23] Lee W-P, Yang K-C. A clustering-based approach for inferring recurrent neural networks as gene regulatory networks. *Neurocomputing* 2008;71:600–10.
- [24] Liu L-Z, Wu F-X, Zhang W-J. Inference of biological s-system using the separable estimation method and the genetic algorithm. *IEEE/ACM Trans Comput Biol Bioinform (TCBB)* 2012;9:955–65.
- [25] Lubeck E, Long C. Single-cell systems biology by super-resolution imaging and combinatorial labeling. *Nat Methods* 2012;9:743–50.
- [26] Miller C, Schwalb B, Maier K, Schulz D, Dümcke S, Zacher B, et al. Dynamic transcriptome analysis measures rates of mrna synthesis and decay in yeast. *Mol Syst Biol* 2011;7(1).
- [27] Milo R, Shen-Orr S, Itzkovitz S, Kashtan N, Chklovskii D, Alon U. Network motifs: simple building blocks of complex networks. *Science* 2002;298(5594):824–7.
- [28] Monod J, Jacob F. General conclusions: teleonomic mechanisms in cellular metabolism, growth, and differentiation. *Cold Spring Harb Symp Quant Biol* 1961;26:389–401.
- [29] Oltvai ZN, Barabasi A-L. Life's complexity pyramid. *Science* 2002;298:763–4.
- [30] Ozbudak E, Thattai M, Lim N, Shraiman B, van Oudenaarden A. Multistability in the lactose utilization network of *escherichia coli*. *Nature* 2004;427:737–40.
- [31] Pan X, Heitman J. Sok2 regulates yeast pseudohyphal differentiation via a transcription factor cascade that regulates cell-cell adhesion. *Mol Cell Biol* 2000;20:83648372.
- [32] Savageau M. *Biochemical system analysis: a study of function and design in molecular biology*. Addison-Wesley; 1976.
- [33] Stathopoulos A, Cyert M. Calcineurin acts through the *crz1/tcn1*-encoded transcription factor to regulate gene expression in yeast. *Genes Dev* 1997;11:3432–44.
- [34] Swain MT, Mandel JJ, Dubitzky W. Comparative study of three commonly used continuous deterministic methods for modeling gene regulation networks. *BMC Bioinform* 2010;11:459.
- [35] Tan C, Marguet P, You L. Emergent bistability by a growth-modulating positive feedback circuit. *Nat Chem Biol* 2009;5(11):842–8.
- [36] To CC, Vohradsky J. Measurement variation determines the gene network topology reconstructed from experimental data: a case study of the yeast cyclin network. *FASEB J Res Commun* 2010;24:3468–78.
- [37] Vachova L, Devaux F, Kucerova H, Ricicova M, Jacq C, Palkova Z. Sok2p transcription factor is involved in adaptive program relevant for long term survival of *saccharomyces cerevisiae* colonies. *J Biol Chem* 2004;279:37973–81.
- [38] Ventura AC, Jiang P, Van Wassenhove L, Del Vecchio D, Merajver SD, Ninfa AJ. Signaling properties of a covalent modification cycle are altered by a downstream target. *Proc Natl Acad Sci* 2010;107(22):10032–7.
- [39] Vohradská E, Vohradsky J. Virtual mutagenesis of the yeast cyclins genetic network reveals complex dynamics of transcriptional control networks. *PLoS ONE* 2011;6:e18827.
- [40] Vohradsky J. Neural network model of gene expression. *FASEB J* 2001;15:846–54.
- [41] Vu TT, Vohradsky J. Genexp - a genetic network simulation environment. *Bioinform Appl Note* 2002;18:1400–1.
- [42] Vu TT, Vohradsky J. Inference of active transcriptional networks by integration of gene expression kinetics modeling and multisource data. *Genomics* 2009;93:426–33.
- [43] Vu T, Vohradsky J. Nonlinear differential equation model for quantification of transcriptional regulation applied to microarray data of *saccharomyces cerevisiae*. *Nucleic Acids Res* 2007;35:279–87.
- [44] Wang Y, Liu CL, Storey JD, Tibshirani RJ, Herschlag D, Brown PO. Precision and functional specificity in mrna decay. *Proc Natl Acad Sci* 2002;99(9):5860–5.
- [45] Yoshimoto H, Saltsman K, Gasch A, Li H, Ogawa N, Botstein D, et al. Genome-wide analysis of gene expression regulated by the calcineurin/*crz1p* signaling pathway in *saccharomyces cerevisiae*. *J Biol Chem* 2002;277:31079–88.